Addition of Metallic Mercury to Platinum− and Palladium−Gold Cluster Compounds. X-ray Crystal and Molecular Structures of $[(Hg)_2Pd(AuPPh_3)_8](NO_3)_2$ and $[(Hg)Pt(AuPPh_3)_8](NO_3)_2$

Rachael A. T. Gould, Kathryn L. Craighead, Jack S. Wiley, and Louis H. Pignolet*

Department of Chemistry, University of Minnesota, Minneapolis, Minnesota 55455

Received January 12, 1995[⊗]

Several new cluster compounds have been prepared by reaction of metallic Hg with the 16-electron clusters $[M(AuPPh_3)_8]^{n+}$ (M = Pt, Pd, n = 2; M = Au, n = 3) to form the 20-electron clusters $[(Hg)_2M(AuPPh_3)_8]^{2+}$ (M = Pt, **1**; Pd, **2**) and $[(Hg)_2Au(AuPPh_3)_8]^{3+}$ (**3**). In contrast, reaction of the 16-electron clusters with Hg_2^{2+} salts gave the 18-electron clusters $[(HgNO_3)_2M(AuPPh_3)_8]^{2+}$ (M = Pt, **6**; Pd, **7**). The 18-electron, monomercury clusters $[(Hg)M(AuPPh_3)_8]^{2+}$ (M = Pt, **4**; Pd, **5**) were isolated as intermediates in the formation of clusters **1** and **2** and were also prepared by reaction of clusters **1** or **2** with 1 equiv of $[M(AuPPh_3)_8]^{2+}$ (M = Pt, Pd). Clusters **1**−**7** have been characterized by spectroscopic and analytical methods, and the nitrate salts of **2** and **4**, by single crystal, X-ray diffraction. The crystal data for these compounds are as follows: for **2**$(NO_3)_2$, orthorhombic *Fddd*, a = 34.66(2) Å, b = 42.09(3) Å, c = 39.29(3) Å, V = 57 329 Å^3, Z = 16, residuals R = 0.099 and R_w = 0.098 for 1777 observed reflections and 152 variables, Mo Kα radiation; for **4**$(NO_3)_2$, monoclinic $P2_1/n$, a = 16.95(2) Å, b = 31.60(3) Å, c = 25.69(3) Å, β = 94.07(7)°, V = 13 725 Å^3, Z = 4, residuals R = 0.088 and R_w = 0.081 for 7504 observed reflections and 441 variables, Mo Kα radiation. The structure of the cluster core of **2**$(NO_3)_2$ is a Pd centered square-antiprism with bare Hg atoms capping the two square faces. A crystal of the Pt analog, **1**$(NO_3)_2$, was isomorphous and presumably isostructural to **2**$(NO_3)_2$. The structure of **4**$(NO_3)_2$ is similar to that of **2**$(NO_3)_2$ with one of the capping Hg atoms removed. A crystal of **5**$(NO_3)_2$ was isomorphous and presumably isostructural to **4**$(NO_3)_2$. The reactions of **1**−**7** with CO, Cl^-, and redox agents have been examined. Importantly, **1** was quantitatively converted into its 18-electron analog **6** by the addition of 2 equiv of $Fe(\eta^5\text{-}C_5H_5)_2^+$, supporting its 20-electron description.

Introduction

The area of heteronuclear gold cluster chemistry has grown enormously over the past decade.[1−4] Phosphine stabilized, high nuclearity, Pt− and Pd−Au cluster compounds that contain Au−M (M = Pt, Pd) and Au−Au bonds have shown a rich chemistry because of their ability to react with a wide variety of substrates and their recently discovered catalytic activation of dihydrogen.[5−8] These clusters are currently being investigated as models for bi- and polymetallic heterogeneous catalysts. Such studies should provide a better understanding of metal−metal bonding and of the synergism often observed in bimetallic catalysis.[1,9] We are interested in developing systematic methods of preparing new heterometallic cluster compounds, especially clusters that contain a third metal. The focus of this paper is on the preparation, characterization, and study of a series of new M−Au clusters that contain Hg.

The structural and reactivity properties of M-centered gold cluster compounds have been rationalized with the use of an electron counting formalism.[1−3,10] The clusters have been classified as having 16 or 18 valence electrons in the cluster core. This includes valence electrons from the central metal and electrons in the inward pointing orbitals of σ symmetry from the peripheral metals or ligands. An example of a 16-electron cluster is $[(PPh_3)Pt(AuPPh_3)_6]^{2+}$. In this cluster, Pt donates 10 electrons, PPh_3 donates 2, each $AuPPh_3$ donates 1 (6 in all), and the 2+ charge takes 2 away for a total of 16. $[Pt(AuPPh_3)_8]^{2+}$ is another example of a 16-electron cluster. All of the heteronuclear gold clusters and homonuclear gold clusters currently known having 18 valence electrons have structures in which the peripheral gold atoms and other central metal bound ligands (such as PPh_3 and CO) have a spheroidal geometry; clusters with 16 valence electrons have flattened or toroidal structures. In general, a 16-electron cluster is reactive toward the addition of one 2-electron donor ligand (such as CO) to form a 18-electron cluster. An example is the reaction of $[M(AuPPh_3)_8]^{2+}$ with CO to give $[M(CO)(AuPPh_3)_8]^{2+}$ where M = Pd or Pt. This electron-counting formalism provides a useful, although simplified, means of classifying the reactions and structures of these clusters.

[⊗] Abstract published in *Advance ACS Abstracts,* May 1, 1995.

(1) Pignolet, L. H.; Aubart, M. A.; Craighead, K. L.; Gould, R. A. T.; Krogstad, D. A.; Wiley, J. S. *Coord. Chem. Rev.* **1995**, in press.
(2) Mingos, D. M. P.; Watson, M. J. *Adv. Inorg. Chem.* **1992**, *39*, 327.
(3) Steggerda, J. J. *Comments Inorg. Chem.* **1991**, *11*, 113.
(4) Teo, B. K.; Keating, K. *J. Am. Chem. Soc.* **1984**, *106*, 2224. Teo, B. K.; Hong, M. C.; Zhang, H.; Huang, D. B. *Angew. Chem., Int. Ed. Engl.* **1987**, *26*, 897. Teo, B. K.; Zhang, H. *Angew. Chem., Int. Ed. Engl.* **1992**, *31*, 445. Teo, B. K.; Zhang, H.; Shi, X. J. Am. Chem. Soc. **1993**, *115*, 8489. Teo, B. K.; Zhang, H.; Shi, X. *Inorg. Chem.* **1994**, *33*, 4086.
(5) Aubart, M. A.; Pignolet, L. H. *J. Am. Chem. Soc.* **1992**, *114*, 7901.
(6) Kappen, T. G. M. M.; Bour, J. J.; Schlebos, P. P. J.; Roelofsen, A. M.; van der Linden, J. G. M.; Steggerda, J. J.; Aubart, M. A.; Krogstad, D. A.; Schoondergang, M. F. J.; and Pignolet, L. H. *Inorg. Chem.* **1993**, *32*, 1074.
(7) Aubart, M. A.; Chandler, B. D.; Gould, R. A. T.; Krogstad, D. A.; Schoondergang, M. F. J.; and Pignolet, L. H. *Inorg. Chem.* **1994**, *33*, 3724.
(8) Aubart, M. A.; Koch, J. F. D.; Pignolet, L. H. *Inorg. Chem.* **1994**, *33*, 3852.
(9) See, for example: *Metal Clusters in Catalysis*; Gates, B. C., Guczi, L., Knözinger, H., Eds.; Elsevier: Amsterdam, 1986; Vol. 29. Lewis, L. N. *Chem. Rev.* **1993**, *93*, 2693. Mingos, D. M. P. *J. Cluster Sci.* **1992**, *3*, 397. Süss-fink, G.; Meister, G. *Adv. Organomet. Chem.* **1993**, *35*, 41. Schwank, J.; Balakrishnan, K.; Sachdev, A. In *New Frontiers in Catalysis*; Guczi, L., Solymosi, F., Tetenyi, P., Eds.; Elsevier: Amsterdam, 1993; p 905.
(10) Mingos, D. M. P.; Wales, D. J. *Introduction to Cluster Chemistry*; Prentice Hall: Englewood Cliffs, NJ, 1993. Mingos, D. M. P.; Johnson, R. L. *Struct. Bonding* **1987**, *88*, 29. Stone, A. J. *Inorg. Chem.* **1981**, *20*, 563.

0020-1669/95/1334-2902$09.00/0

Scheme 1

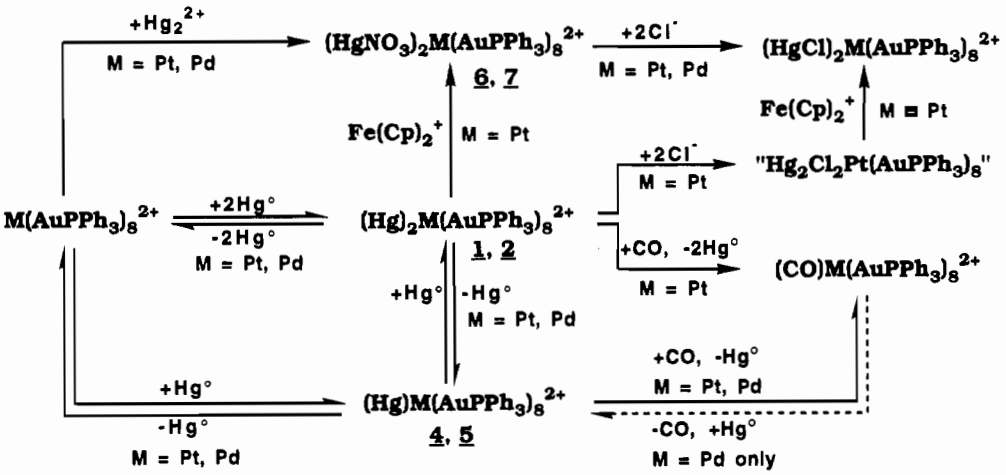

In this paper we compare the reactivity of the 16-electron clusters $[M(AuPPh_3)_8]^{2+}$ (M = Pt or Pd) toward Hg_2^{2+} and metallic Hg. In the former case the 18-electron clusters $[(HgNO_3)_2M(AuPPh_3)_8]^{2+}$ are formed,[11] while in the latter the unexpected, 20-electron clusters $[(Hg)_2M(AuPPh_3)_8]^{2+}$ are formed. The analytical, chemical, and physical properties of these new M−Hg−Au clusters are presented in this paper.

Results

Several new cluster compounds have been prepared *via* the reaction of metallic Hg with the 16-electron clusters $[M(AuPPh_3)_8]^{n+}$ (M = Pt, Pd, n = 2; M = Au, n = 3) to form the 20-electron clusters $[(Hg)_2M(AuPPh_3)_8]^{2+}$ (M = Pt, **1**; Pd, **2**) and $[(Hg)_2Au(AuPPh_3)_8]^{3+}$ (**3**). The counteranions are NO_3^- throughout this paper, unless indicated otherwise. In contrast, reaction of the 16-electron clusters with Hg_2^{2+} salts gave the 18-electron clusters $[(HgNO_3)_2M(AuPPh_3)_8]^{2+}$ (M = Pt, **6**; Pd, **7**). Nitrate anions are bound to the Hg atoms in these compounds in the solution phase (vide infra). The 18-electron, monomercury clusters $[(Hg)M(AuPPh_3)_8]^{2+}$ (M = Pt, **4**; Pd, **5**) were isolated as intermediates in the formation of clusters **1** and **2**, and were also prepared by reaction of clusters **1** and **2** with 1 equiv of the corresponding $[M(AuPPh_3)_8]^{2+}$. The transformations observed in this study for M = Pt, Pd are summarized in Scheme 1 and described in the Experimental Section. Clusters **1**−**7** have been characterized by spectroscopic and analytical methods, and the nitrate salts of **2** and **4**, by single-crystal X-ray diffraction. Characterization data for all new clusters are included in the Experimental Section and are discussed below when appropriate. Cluster **6** has been reported previously and characterized by X-ray diffraction.[11]

Compounds **1**−**3** are unusual in that they can be classified as 20-electron clusters. Their reactivity properties are distinctly different from those of the 18-electron clusters **6** and **7**. For example, clusters **6** and **7** reacted stoichiometrically with 2 equiv of Cl^- to form $[(HgCl)_2M(AuPPh_3)_8]^{2+}$. In contrast, the reactivity of the 20-electron clusters **1** and **2** with Cl^- was complicated. The Pt-centered cluster **1** reacted with Cl^- to form an insoluble orange solid believed to have the formulation "$Hg_2Cl_2Pt(AuPPh_3)_8$", while the Pd analog **2** did not react with Cl^-. This 20-electron cluster "$Hg_2Cl_2Pt(AuPPh_3)_8$" was subsequently oxidized to the 18-electron cluster $[(HgCl)_2M(AuPPh_3)_8](PF_6)_2$ by reaction with $[Fe(\eta^5\text{-}C_5H_5)_2]PF_6$, although this reaction was not clean. In a similar manner, **1** was converted into $\mathbf{6}(PF_6)_2$ quantitatively by the addition of 2 equiv of $[Fe(\eta^5\text{-}C_5H_5)_2]PF_6$. These transformations and others shown in the Scheme 1 provide support for the 20-electron description of **1**−**3**.

Crystal Structure of $[(Hg)_2Pd(AuPPh_3)_8](NO_3)_2$, $\mathbf{2}(NO_3)_2$. A summary of crystal data is presented in Table 1. Positional and thermal parameters of atoms in the cluster core are given in Table 2. Complete crystallographic data are included as supplementary material.[12] The molecular structure of the cluster core along with the crystallographic labeling scheme and some selected distances are shown in Figure 1. ^{31}P NMR data verify that the metal atoms connected to PPh_3 ligands are Au, and the bare metal atoms capping Au_4 faces are Hg (vide infra). This is in agreement with the other Hg adducts of PtAu clusters which have been structurally characterized.[11,13,14]

The $PdAu_8Hg_2$ framework of the 20-electron cluster $\mathbf{2}(NO_3)_2$ is very similar to that reported in the literature for a crystal of the 18-electron, Pt-centered cluster formulated as $[(Hg)_2Pt(AuPPh_3)_8](NO_3)_4$.[11] The cluster $[(Hg)_2Pt(AuPPh_3)_8](NO_3)_4$ has bare Hg atoms and therefore was assumed to be a tetracation in the solid state; however, the NO_3^- ions were not located due to disorder and the presence of disordered solvent of crystallization.[11] In solution it was formulated as $[(HgNO_3)_2Pt(AuPPh_3)_8](NO_3)_2$ from conductivity measurements, and therefore equivalent to $\mathbf{6}(NO_3)_2$ in this paper. It is possible that the crystal structure of $[(Hg)_2Pt(AuPPh_3)_8](NO_3)_4$ reported in the literature[11] is actually that of the 20-electron cluster $\mathbf{1}(NO_3)_2$, a possible contaminant in samples of $\mathbf{6}(NO_3)_2$. This is especially likely due to the close similarity of the structures of **2** and **6** (vide infra and Table 3). Numerous attempts to grow X-ray quality crystals from pure samples of $\mathbf{6}(NO_3)_2$ under conditions identical to those described in the literature[11] were unsuccessful. Here we will refer to this compound as $[(Hg)_2Pt(AuPPh_3)_8](NO_3)_4$ with the understanding that it may actually be $\mathbf{1}(NO_3)_2$.

Crystallographic 2-fold molecular symmetry was observed for $\mathbf{2}(NO_3)_2$ while $[(Hg)_2Pt(AuPPh_3)_8](NO_3)_4$ had 4-fold symmetry. The symmetry in both clusters is however, close to 8-fold rotation inversion. The centered square-antiprismatic geometry of $[(Hg)_2Pt(AuPPh_3)_8](NO_3)_4$ and $\mathbf{2}(NO_3)_2$ is similar to that of the parent $[Pd(AuPPh_3)_8](NO_3)_2$ cluster,[16] with Hg atoms capping the two square faces. A comparison of some of

(11) Bour, J. J.; van der Berg, W.; Schlebos, P. P. J.; Kanters, R. P. F.; Schoondergang, M. F. J.; Bosman, W. P.; Smits, J. M. M.; Beurskens, P. T.; Steggerda, J. J.; van der Sluis, P. *Inorg. Chem.* **1990**, *29*, 2971.

(12) See paragraph at the end of the paper regarding supplementary material.

(13) Gould, R. A. T.; Pignolet, L. H. *Inorg. Chem.* **1994**, *33* , 40.

(14) Ito, L. N.; Felicissimo, A. M. P.; Pignolet, L. H. *Inorg. Chem.* **1991**, *30*, 387.

(15) Bour, J. J.; Kanters, R. P. F.; Schlebos, P. P. J.; Steggerda, J. J. *Recl.: J. R. Neth. Chem. Soc.* **1988**, *107*, 211.

Table 1. Crystallographic Data for $2(NO_3)_2$ and $4(NO_3)_2$

	$2(NO_3)_2$	$4(NO_3)_2$
Crystal Parameters and Measurement of Intensity Data		
cryst syst	orthorhombic	monoclinic
space group	*Fddd* (No. 70)	$P2_1/n$ (No. 14)
crystal dimens	0.40 × 0.40 × 0.30	0.30 × 0.20 × 0.15
cell params		
T, °C	+24	+24
a, Å	34.66(2)	16.95(2)
b, Å	42.09(3)	31.60(3)
c, Å	39.29(3)	25.69(3)
β, deg		94.07(7)
V, Å^3	57,329	13,725
Z	16	4
calcd density, g cm^{-3}	1.995	2.029
abs coeff, cm^{-1}	105.27	107.72
max, min transm factors	0.71, 1.40	0.36, 1.00
formula	$C_{144}H_{120}N_2O_6P_8Au_8PdHg_2$	$C_{144}H_{120}N_2O_6P_8Au_8PtHg$
fw, amu	4305.67	4193.74
diffractometer	CAD 4	CAD 4
radiation	Mo Kα (λ = 0.710 69 Å)	Mo Kα (λ = 0.710 69 Å)
scan type; range (2θ), deg	ω scan; 0−34	ω scan; 0−44
no. of unique rflns measd	4945	16845
no. of obsd rflns[a]	1777 [$I > 2.0\sigma(I)$]	7504 [$I > 2.0\sigma(I)$]
Refinement by Full-Matrix Least Squares		
no. of parames	152	441
R[a]	0.099	0.088
R_w[a]	0.098	0.081
GOF[a]	2.01	1.63
p[a]	0.03	0.03

[a] The function minimized was $\sum w(|F_o| - |F_c|)^2$, where $w = 4F_o^2/s^2(F_o^2)$ and $\sigma^2(F_o^2) = [S^2(C + R^2 + B) + (pF_o^2)^2]/Lp^2$, S = scan rate, C = total integrated peak count, R = ratio of scan time to background counting time, B = total background count, Lp = Lorentz−polarization factor, and p = p-factor used to downweight intense reflections. The unweighted and weighted residuals are defined as $R = \sum(||F_o| - |F_c||)/\sum|F_o|$ and $R_w = [(\sum w(|F_o| - |F_c|)^2)/(\sum w|F_o|^2)]^{1/2}$. The error in an observation of unit weight (GOF) is $[\sum w(|F_o| - |F_c|)^2/(N_o - N_v)]^{1/2}$, where N_o and N_v are the number of observations and variables, respectively.

Table 2. Positional and Thermal Parameters for the Core Atoms in $2(NO_3)_2$[a]

atom	*x*	*y*	*z*	*B*, Å^2
Pd1	1/8	1/8	0.3802 (3)	2.4 (6)
Hg1	1/8	1/8	0.3061 (1)	4.7 (4)
Hg2	1/8	1/8	0.4562 (2)	4.8 (4)
Au1	0.1940 (1)	0.1270 (2)	0.3521 (1)	4.0 (3)
Au2	0.1775 (1)	0.0903 (1)	0.4117 (1)	3.4 (3)
Au3	0.1357 (1)	0.0685 (1)	0.3532 (1)	3.9 (3)
Au4	0.1702 (2)	0.1680 (1)	0.4079 (1)	4.1 (3)
P1	0.243 (1)	0.135 (1)	0.3145 (8)	5 (1)
P2	0.211 (1)	0.061 (1)	0.4501 (8)	4.6 (9)
P3	0.146 (1)	0.028 (1)	0.3206 (8)	4.8 (9)
P4	0.204 (1)	0.201 (1)	0.4446 (8)	4.6 (9)

[a] Parameters for the remaining atoms in the structure are included as supplementary material.[12] Anisotropically refined atoms are given in the form of the isotropic equivalent thermal parameter defined as $(4/3)[a^2\beta(1,1) + b^2\beta(2,2) + c^2\beta(3,3) + ab(\cos\gamma)\beta(1,2) + ac(\cos\beta)\beta(1,3) + bc(\cos\alpha)\beta(2,3)]$.

the bond distances in $[(Hg)_2Pt(AuPPh_3)_8](NO_3)_4$ and $2(NO_3)_2$ is shown in Table 3. The Pd−Hg bond distances in $2(NO_3)_2$ are 2.91 and 2.98 Å and are similar to the Pt−Hg distances in $[(Hg)_2Pt(AuPPh_3)_8](NO_3)_4$ (2.928, 3.045 Å).[11] These distances

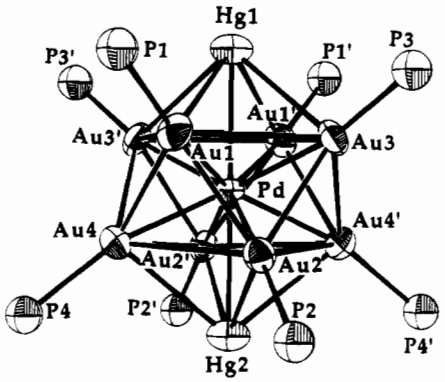

Figure 1. ORTEP drawing of the coordination core of $2(NO_3)_2$. Ellipsoids are drawn with 50% probability boundaries, and phenyl rings have been omitted for the sake of clarity. Atoms labeled with a prime are related to their unprimed counterparts by a crystallographic 2-fold axis that passes through the Hg and Pd atoms. Selected distances in Å and their esd's between the metals in the core of **2** are as follows. Hg1−Au1 3.000(6); Hg1−Au1′ 3.000(6); Hg1−Au3 3.036(7); Hg1−Au3′ 3.038(7); Hg2−Au2 2.915(7); Hg2−Au2′ 2.916(7); Hg2−Au4 3.055(7); Hg2−Au4′ 3.056(7); Pd−Hg1 2.91(1); Pd−Hg2 2.98(1); Pd−Au1 2.638(6); Pd−Au1′ 2.638(6); Pd−Au3 2.633(7); Pd−Au3′ 2.634(7); Pd−Au4 2.630(7); Pd−Au4′ 2.630(7); Au1−Au2 2.863(8); Au1−Au4 2.908(8); Au1−Au3 3.188(8); Au1−Au3′ 3.594(8); Au2−Au3 2.869(7); Au2−Au4 3.282(8); Au2−Au4′ 3.410(8); Au3−Au4 2.951(7).

are significantly longer than in the other known Pt−Au−Hg clusters $[(HgNO_3)_2(PPh_3)Pt(AuPPh_3)_5]^+$ and $[(HgNO_3)(PPh_3)Pt(AuPPh_3)_6]^+$ (2.651−2.684 Å) where the Hg atoms occupy icosahedral vertex positions in the cluster cores.[13,14] The nearest neighbor Hg−Au distances within the core of $2(NO_3)_2$ are similar to values found in the PtAuHg clusters.[11,13,14] The nearest Au−Au distances in $2(NO_3)_2$ and $[(Hg)_2Pt(AuPPh_3)_8](NO_3)_4$ are significantly longer than in $[Pt(AuPPh_3)_8](NO_3)_2$ or $[Pd(AuPPh_3)_8](NO_3)_2$ (average 2.792 Å).[15,16] The Pd−Au distances in $2(NO_3)_2$ are similar to Pt-Au distances in the PtAuHg clusters (Table 3) and are within the range of values observed in PdAu clusters containing primarily phosphine ligands. The Au−P bond lengths are also in the range normally found in gold and mixed-metal gold clusters.[1−4,19] In $[(Hg)_2Pt(AuPPh_3)_8](NO_3)_4$ and $2(NO_3)_2$ the capping Hg atoms have no close contacts with NO_3^- or solvent molecules. This result is in agreement with IR data showing no bound NO_3^- stretches at ca. 1260 cm^{-1}.

Unit Cell Determination of $[(Hg)_2Pt(AuPPh_3)_8](NO_3)_2$, $1(NO_3)_2$. Red crystals of $1(NO_3)_2$ were isolated in two polymorphic forms, neither of which were suitable for a complete X-ray structure determination. One form was isomorphous and presumably isostructural with its Pd analog, $2(NO_3)_2$, {space group *Fddd*; a = 34.38(4) Å, b = 41.20(2) Å, c = 38.48(2) Å, V = 54500 Å^3}. The other form was isomorphous and probably isostructural with $[(Hg)_2Pt(AuPPh_3)_8](NO_3)_4$ {unit cell of $1(NO_3)_2$ is in space group $P4/n$, a = 17.656 Å, c = 22.812 Å, V = 7111 Å^3; unit cell of $[(Hg)_2Pt(AuPPh_3)_8](NO_3)_4$[11] is in space group $P4/n$, a = 17.8002(6) Å, c = 23.0493(13) Å, V = 7303 Å^3}. The difference in unit cell volume between the above crystals is probably due to differences in the solvate molecules, which are usually disordered and loosely bound in these structures. ^{31}P NMR analysis of solutions from

(16) Ito, L. N.; Johnson, B. J.; Mueting, A. M.; Pignolet, L. H. *Inorg. Chem.* **1989**, *28*, 2026.

(17) Ito, L. N.; Felicissimo, A. M. P.; Pignolet, L. H. *Inorg. Chem.* **1991**, *30*, 988.

(18) Craighead, K. L.; Felicissimo, A. M. P.; Krogstad, D. A.; Nelson, L. T. J.; Pignolet, L. H. *Inorg. Chim. Acta* **1993**, *212*, 31.

(19) Schoondergang, M. F. J.; Bour, J. J.; Schlebos, P. P. J.; Vermeer, A. W. P.; Bosman, W. P.; Smits, J. M. M.; Beurskens, P. T.; Steggerda, J. J. *Inorg. Chem.* **1991**, *30*, 4704 and references cited therein.

Table 3. Comparison of Selected Distances (Å)[a] in M−Au−Hg Cluster Compounds (M = Pt, Pd)

	$[Pt(AuPPh_3)_8](NO_3)_2$[c]	$[(Hg)_2Pt(AuPPh_3)_8](NO_3)_4$[d]	$[(Hg)_2Pd(AuPPh_3)_8](NO_3)_2$, **2(NO$_3$)$_2$**	$[(Hg)Pt(AuPPh_3)_8](NO_3)_2$, **4(NO$_3$)$_2$**
Hg−M		2.928, 3.045	2.91, 2.98	2.810
Hg−Au		3.004 (3.007−3.001)	3.002 (2.915−3.056)	3.018 (3.079−2.979)
M−Au (all)	2.635	2.632	2.636	2.629
M−Au (top)[b]	2.640, 2.638	2.632	2.638, 2.633	2.622 (2.611−2.639)
M−Au (bottom)	2.626, 2.636	2.631	2.641, 2.630	2.636 (2.616−2.654)
Au−Au (all)	3.031	3.135	3.133	3.123
Au−Au (top)[b]	3.200	3.380	3.391 (3.188−3.594)	3.420 (3.227−3.641)
Au−Au (bottom)[b]	3.474	3.325	3.346 (3.282−3.410)	3.300 (3.183−3.441)
Au−Au (top-bottom)[b]	2.827 (2.800−2.864)	2.917 (2.904−2.930)	2.898 (2.863−2.951)	2.885 (2.820−2.944)
Au−P (all)	2.27 (2.26−2.28)	2.29 (2.295−2.289)	2.26 (2.17−2.33)	2.28 (2.24−2.32)

Table 4. Positional and Thermal Parameters for the Core Atoms in **4(NO$_3$)$_2$**[a]

atom	*x*	*y*	*z*	*B*, Å^2
Hg	0.7121 (2)	0.11269 (8)	0.8062 (1)	5.2 (1)
Au1	0.6205 (1)	0.18856 (6)	0.83896 (8)	3.5 (1)
Au2	0.5353 (2)	0.09797 (6)	0.8203 (1)	3.9 (1)
Au3	0.6267 (1)	0.07920 (6)	0.70954 (9)	3.7 (1)
Au4	0.7197 (1)	0.17542 (7)	0.7189 (1)	4.0 (1)
Au5	0.4609 (1)	0.17919 (7)	0.79887 (9)	3.7 (1)
Au6	0.4608 (1)	0.10356 (6)	0.71707 (9)	3.5 (1)
Au7	0.5902 (1)	0.15348 (7)	0.64914 (8)	3.3 (1)
Au8	0.5918 (1)	0.23400 (6)	0.73940 (9)	3.5 (1)
Pt	0.5822 (1)	0.15069 (6)	0.75041 (8)	2.6 (1)
P1	0.690 (1)	0.2084 (5)	0.9143 (6)	4.9 (9)
P2	0.523 (1)	0.0550 (5)	0.8912 (6)	4.2 (8)
P3	0.695 (1)	0.0197 (4)	0.6887 (6)	4.2 (8)
P4	0.852 (1)	0.1809 (5)	0.7073 (6)	4.4 (8)
P5	0.346 (1)	0.2105 (5)	0.8154 (6)	4.1 (8)
P6	0.343 (1)	0.0776 (4)	0.6836 (6)	4.0 (8)
P7	0.578 (1)	0.1663 (5)	0.5631 (6)	3.8 (7)
P8	0.579 (1)	0.3061 (4)	0.7244 (6)	4.7 (8)

[a] Parameters for the remaining atoms in the structure are included as supplementary material.[12] Anisotropically refined atoms are given in the form of the isotropic equivalent thermal parameter defined as $(4/3)[a^2\beta(1,1) + b^2\beta(2,2) + c^2\beta(3,3) + ab(\cos\gamma)\beta(1,2) + ac(\cos\beta)\beta(1,3) + bc(\cos\alpha)\beta(2,3)]$.

both crystal forms of **1(NO$_3$)$_2$**, however, support the formulation of these crystals as the 20-electron cluster $[(Hg)_2Pt(AuPPh_3)_8](NO_3)_2$, with no traces of **6(NO$_3$)$_2$** (vide infra).

Crystal Structure of $[(Hg)Pt(AuPPh_3)_8](NO_3)_2$, 4(NO$_3$)$_2$. A summary of the crystal data for **4(NO$_3$)$_2$** is presented in Table 1. The unit cell determination of crystals of the Pd analog, **5(NO$_3$)$_2$**, {space group $P2_1/n$; a = 17.01(1) Å, b = 31.718(6) Å, c = 25.78(2) Å, β = 94.32(6)°, V = 13868(67) Å^3} shows it to be isomorphous and presumably isostructural to **4(NO$_3$)$_2$**, so no further data was collected on crystals of **5(NO$_3$)$_2$**. Positional and thermal parameters of atoms in the cluster core are given for **4(NO$_3$)$_2$** in Table 4. The molecular structure of the cluster core with the crystallographic labeling scheme and some selected distances are given in Figures 2 and 3. The ^{31}P NMR data indicates that the Pt atom is in the center of the $PtAu_8$-Hg skeleton, the metal atoms connected to PPh_3 ligands are Au, and the capping metal atom is Hg (vide infra). This is consistent with other Hg adducts of PtAu clusters.[11,13,14]

The cluster core of **4(NO$_3$)$_2$** is similar to that of **2(NO$_3$)$_2$** with one of the capping Hg atoms removed. The structure of **4(NO$_3$)$_2$** is the first example of a monocapped square antiprism geometry for an 18-electron MAu cluster compound. The metal−metal bond distances in **4(NO$_3$)$_2$** are compared to those of the bicapped Hg clusters $[(Hg)_2Pt(AuPPh_3)_8](NO_3)_4$ and **2(NO$_3$)$_2$** in Table 3. The Au−Au, M−Au, and Hg−Au distances are similar in all three structures, although those in **4(NO$_3$)$_2$** are slightly shorter. The Pt−Hg bond in **4(NO$_3$)$_2$**, however, is significantly shorter (2.810 Å) than the Hg−M bonds in $[(Hg)_2Pt(AuPPh_3)_8](NO_3)_4$ and **2(NO$_3$)$_2$**, which average 2.987 and 2.95 Å, respectively. The Pt−Au distances in **4(NO$_3$)$_2$** are similar to values in the other PtAuHg clusters and are within the range of values observed in PtAu clusters containing primarily phosphine ligands.[1-4,19] The Au−P bond lengths are also in the range normally found in gold and mixed-metal gold clusters. As with $[(Hg)_2Pt(AuPPh_3)_8](NO_3)_4$ and **2(NO$_3$)$_2$**, no electron density was found in difference Fourier maps within a bonding distance of the Hg atom. This was confirmed by the absence of bound NO_3^- stretches (ca. 1260 cm^{-1}) in the IR.

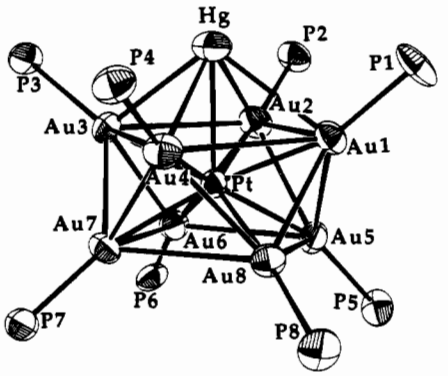

Figure 2. ORTEP drawing of the cluster core of **4(NO$_3$)$_2$**. Ellipsoids are drawn with 50% probability boundaries, and phenyl rings have been omitted for the sake of clarity. Selected distances in Å and their esd's between the metals in the cluster core of **4(NO$_3$)$_2$** are as follows. Hg−Pt 2.810(4); Hg−Au3 2.979(5); Hg−Au4 3.004(4); Hg−Au1 3.008(4); Hg−Au2 3.079(5); Pt−Au1 2.611(4); Pt−Au2 2.615(4); Pt−Au3 2.614(3); Pt−Au4 2.639(4); Pt−Au5 2.637(4); Pt−Au6 2.635(4); Pt−Au7 2.616(4); Pt−Au8 2.654(4); Au1−Au5 2.841(5); Au1−Au8 2.944(4); Au1−Au2 3.227(4); Au1−Au4 3.641(5); Au2−Au6 2.861(5); Au2−Au5 2.895(4); Au2−Au3 3.388(5); Au3−Au7 2.857(4); Au3−Au6 2.936(5); Au3−Au4 3.425(4); Au4−Au7 2.820(4); Au4−Au8 2.928(4); Au5−Au6 3.183(4); Au5−Au8 3.276(4); Au6−Au7 3.300(4); Au7−Au8 3.441(4).

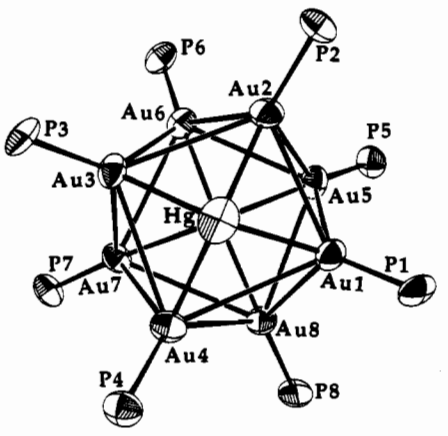

Figure 3. Top view ORTEP drawing of the cluster core of **4(NO$_3$)$_2$** looking down the Hg-Pt axis. Note the approximate 4-fold symmetry.

Synthesis and Characterization. $[(Hg)_2M(AuPPh_3)_8]^{2+}$ (M = Pt, 1; Pd, 2). Clusters **1** and **2** were prepared by reaction of

Table 5. Spectroscopic and Analytical Data for **1**−**7**

compound	Λ, mho cm^{-1} mol^{-1} (solvent)	IR $\nu(NO_3)$, cm^{-1} (CsI pellets)	% N calcd, obsd
$Pt(AuPPh_3)_8(NO_3)_2$	313 (acetone)	1360 (br)	
$(Hg)_2Pt(AuPPh_3)_8(NO_3)_2$, **1**$(NO_3)_2$	310 (acetone)	1357 (br)	0.64, 0.62
$(Hg)_2Pd(AuPPh_3)_8(NO_3)_2$, **2**$(NO_3)_2$	304 (CH_3CN)	1363 (br)	0.65, 0.66
$(Hg)_2Au(AuPPh_3)_8(NO_3)_3$, **3**$(NO_3)_3$	378 (CH_3CN)	1348 (br)	0.94, 1.06
$(Hg)Pt(AuPPh_3)_8(NO_3)_2$, **4**$(NO_3)_2$	312 (CH_3CN)	1357 (br)	0.67, 0.70
$(Hg)Pd(AuPPh_3)_8(NO_3)_2$, **5**$(NO_3)_2$	304 (CH_3CN)	1357 (br)	0.68, 0.70
$(Hg)_2Pt(AuPPh_3)_8(NO_3)_2(BF_4)_2$, **6**$(NO_3)_2(BF_4)_2$	299 (acetone)	1258 (s); $\nu(BF_4)$ 1058 (s)	
$(HgNO_3)_2Pt(AuPPh_3)_8(NO_3)_2$, **6**$(NO_3)_2$	277 (acetone)[a]	1260 (s), 1360 (br)[b]	1.24, 1.17
$(HgNO_3)_2Pd(AuPPh_3)_8(NO_3)_2$, **7**$(NO_3)_2$	273 (CH_3CN)	1265 (s); 1350 (br)	1.26, 1.32

[a] A larger value, (>500) was reported for this compound in ref 11. [b] Data reported for the polymorph which crystallized as yellow needles.

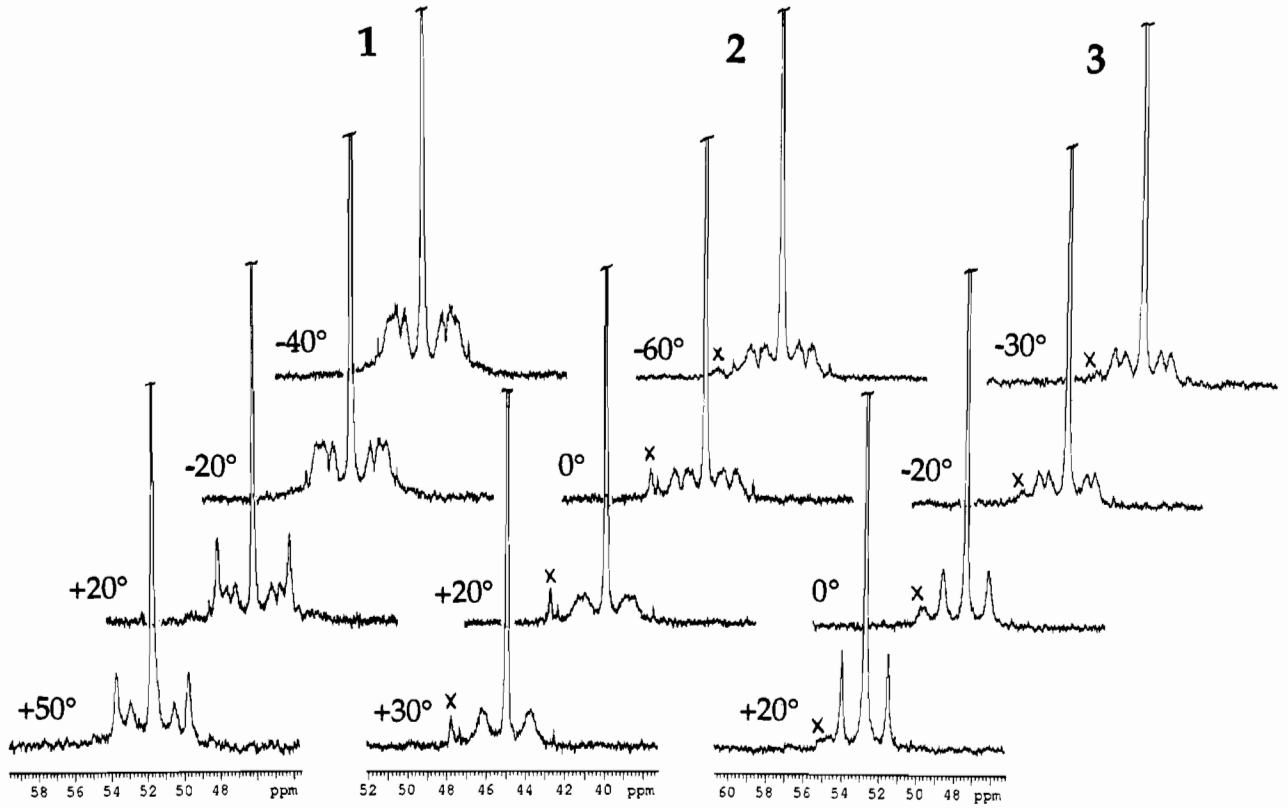

Figure 4. Variable temperature ^{31}P NMR spectra for clusters **1**$(NO_3)_2$ {T = +50 °C in DMSO; T = +20 to −40 °C in CD_3OD}, **2**$(NO_3)_2$ {T = +30 to −60 °C in acetone-d_6}, and **3**$(NO_3)_3$ {T = +20 to −30 °C in CD_3OD}. See Figure 5 and the Experimental Section for an explanation of the coupling patterns. Peaks × are due to the impurity $[Au(AuPPh_3)_8]^{3+}$.

$[M(AuPPh_3)_8]^{2+}$ with metallic mercury. Both reactions gave red, crystalline solids in good yield. IR spectra of **1**$(NO_3)_2$ and **2**$(NO_3)_2$ in the solid state showed the presence of only uncoordinated NO_3^- ions, and elemental analyses and equivalent conductance measurements confirmed the presence of two NO_3^- counterions per cluster (Table 5). IR analysis of the metathesized cluster **1**$(PF_6)_2$ indicated only the presence of PF_6^- and no NO_3^- ions. The fragmentation pattern in the FABMS supported this formulation.

The ^{31}P NMR spectra for **1** and **2** at various temperatures are shown in Figure 4. In the case of **1**, the ^{31}P NMR spectra indicates the presence of one Pt and two Hg atoms. This can be shown by an analysis of the possible isotopomers. A list of the isotopomers and their calculated abundance together with the simulated and actual room temperature ^{31}P NMR spectrum of **1** is shown in Figure 5 and discussed in the Experimental Section. The ^{31}P NMR spectrum of cluster **1** is complicated by coupling to ^{195}Pt (I = $^1/_2$), and ^{199}Hg (I = $^1/_2$) with natural abundance of 33.8 and 16.8%, respectively. A simpler coupling pattern consistent with the presence of two Hg atoms is observed for the Pd-centered cluster **2**. An interpretation of the coupling patterns observed in the variable temperature ^{31}P NMR spectra for these clusters is provided in the Discussion.

The possibility of cluster hydride ligands in **1** and **2** was thoroughly explored using crystallographic, analytical, and spectroscopic methods. No indication of distortions due the presence of hydrido ligands was found in the X-ray structure for **2**$(NO_3)_2$, and no evidence for hydride ligands (either terminal or bridging) was observed in the FTIR, FABMS, ^{31}P NMR, and ^1H NMR spectra. Clusters **1** and **2** prepared with fully deuterated solvents also showed no signals in the ^2H NMR. These NMR experiments were carried out at a variety of temperatures and at 300 and 500 MHz. The instability and low solubility of **1**$(NO_3)_2$ in solution thwarted attempts to find a signal in the ^{195}Pt NMR (chemical shift range −3600 to −7800). Due to the high molecular weights of the clusters, elemental analyses were inconclusive as to the presence of hydrido ligands. In contrast, the hydrido ligands of all known Pt−Au hydrido clusters were readily observed by ^1H NMR.[1,6-8,20-22] The

(20) Kanters, R. P. F.; Bour, J. J .; Schlebos, P. P. J.; Bosman, W. P.; Behm, H. J.; Steggerda, J. J.; Ito, L. N.; Pignolet, L. H. *Inorg. Chem.* **1989**, *28*, 2591.

Possible Isotopomers		Calculated Abundance
*P Pt Hg Hg	(a)	45.76%
*P *Pt Hg Hg	(b)	23.40%
*P Pt *Hg Hg	(c)	18.54%
*P *Pt *Hg Hg	(d)	9.46%
*P Pt *Hg *Hg	(e)	1.88%
*P *Pt *Hg *Hg	(f)	0.96%

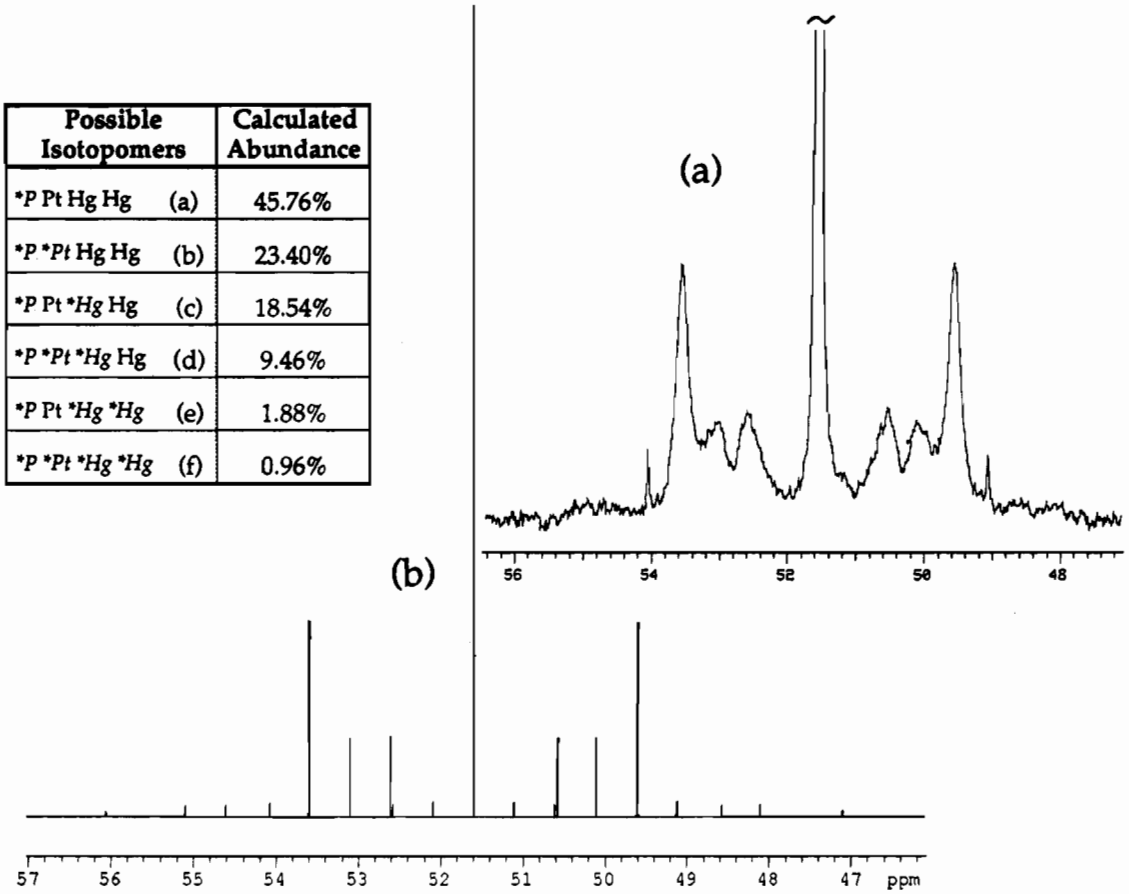

Figure 5. Experimental (a) and simulated (b) ^{31}P NMR spectra for $\mathbf{1}(NO_3)_2$ at ambient temperature demonstrating the superposition of the $^{199}Hg-^{31}P$ and $^{195}Pt-^{31}P$ coupling in the various isotopomers present (see Experimental Section for details). The natural abundances of the spin-active ^{195}Pt ($I = 1/2$) and ^{199}Hg ($I = 1/2$) isotopes are 33.8 and 16.84%, respectively. Spin-active nuclei are marked with an asterisk, and the J values used are given in the Experimental Section for cluster **1**.

absence of NMR detection was therefore taken as strong evidence that **1** and **2** do not contain hydride ligands. The other results presented in this paper (e.g. Scheme 1) are also consistent with this conclusion.

$[(Hg)_2Au(AuPPh_3)_8]^{3+}$ (3). The 16-electron, homometallic gold cluster $[Au(AuPPh_3)_8]^{3+}$ reacted with metallic mercury to form the 20-electron, Au centered bis(mercury) cluster **3**. Although solutions of **3** were light sensitive and gave Au^0 mirrors over time, small red, plate-like crystals were obtained in high yield. IR spectroscopy in the solid state indicated only uncoordinated NO_3^- stretches (ca. 1350 cm^{-1}). The equivalent conductance of **3** in acetone solution (378 mho cm^{-1} mol^{-1}) indicated a 1:3 electrolyte. The FABMS of **3** showed only peaks corresponding to fragmentation of $[Au(AuPPh_3)_8]^{3+}$. This is typical of Au-centered clusters where parent molecular ions are not observed by FABMS.[23] ICP and elemental analysis data confirmed the presence of nine gold atoms, eight phosphine ligands, and two Hg atoms. The variable temperature ^{31}P NMR data (Figure 4) showed that **3** is very similar in dynamic behavior to the 20-electron clusters **1** and **2**. This is discussed further below.

Cluster **3** was unreactive toward CO in contrast to **1**, which reacted giving the known CO adduct $[(CO)Pt(AuPPh_3)_8]^{2+}$ and metallic Hg (see Discussion). This is not surprising since there are no known CO adducts of Au-centered clusters, and Au is not very reactive toward CO.[24] Cluster **3** did react with Cl^- ions to form a compound that may be "$[Hg_2Cl_2Au(AuPPh_3)_8]^+$" by analogy to the Cl^- adduct of **1**; however this cluster was unstable, difficult to isolate, and not further characterized.

$[(Hg)M(AuPPh_3)_8]^{2+}$ (M = Pt, 4; Pd, 5). The monocapped Hg clusters **4** and **5** were formed by reaction of **1** and **2** with a stoichiometric amount of $[M(AuPPh_3)_8]^{2+}$. Both reactions gave dark, X-ray quality crystals in high yield. These clusters were also isolated as intermediates in the synthesis of **1** and **2** from the reaction of $[M(AuPPh_3)_8]^{2+}$ with excess Hg^0. IR spectra of **4** and **5** (Table 5) indicated only uncoordinated NO_3^-, and FABMS, ICP, and elemental analyses confirmed the (Hg)M-$(AuPPh_3)_8(NO_3)_2$ formulation. In solution, crystals of these monomercury clusters dissolved to give equilibrium amounts of the $[M(AuPPh_3)_8]^{2+}$ and $[(Hg)_2M(AuPPh_3)_8]^{2+}$. This was readily observed by ^{31}P NMR (Figure 6). At 20 °C, **4** was observed in the ^{31}P NMR as a broad resonance centered at ca. 57.6 ppm. Sharp peaks due to **1** and $[Pt(AuPPh_3)_8]^{2+}$ were also observed in this spectrum. These resonances and their relative integrals were reproducible for different preparations of **4**. As the temperature was lowered to −60 °C, the broad signal of **4** decoalesced to two resonances of equal intensity with ^{195}Pt and ^{199}Hg satellites (δ 62.6 ppm, $^2J_{^{195}Pt-P}$ 330 Hz, $^3J_{^{199}Hg-P}$ 480 Hz; δ 51.5 ppm, $^2J_{^{195}Pt-P}$ 704 Hz, $^3J_{^{199}Hg-P}$ 704 Hz). The peaks due to **1** and $[Pt(AuPPh_3)_8]^{2+}$ remained sharp as the temperature

(21) Bour, J. J.; Schlebos, P. P. J.; Kanters, R. P. F.; Bosman, W. P.; Smits, J. M. M.; Beurskens, P. T.; Steggerda, J. J. *Inorg. Chim. Acta* **1990**, *171*, 177.
(22) Kappen, T. G. M. M. Ph.D. Thesis (ISBN 9037302521), University of Nijmegen, Nijmegen, The Netherlands, 1994.
(23) Boyle, P. D.; Johnson, B. J.; Alexander, B. D.; Casalnuovo, J. A.; Gannon, P. R.; Johnson, S. M.; Larka, E. A.; Mueting, A. M.; Pignolet, L. H. *Inorg. Chem.* **1987**, *26*, 1346.
(24) Puddephatt, R. J. The Chemistry of Gold. In *Topics in Inorganic and General Chemistry*; Clark, R. J. H., Ed.; Elervier: Amsterdam, 1978; Vol. 16.

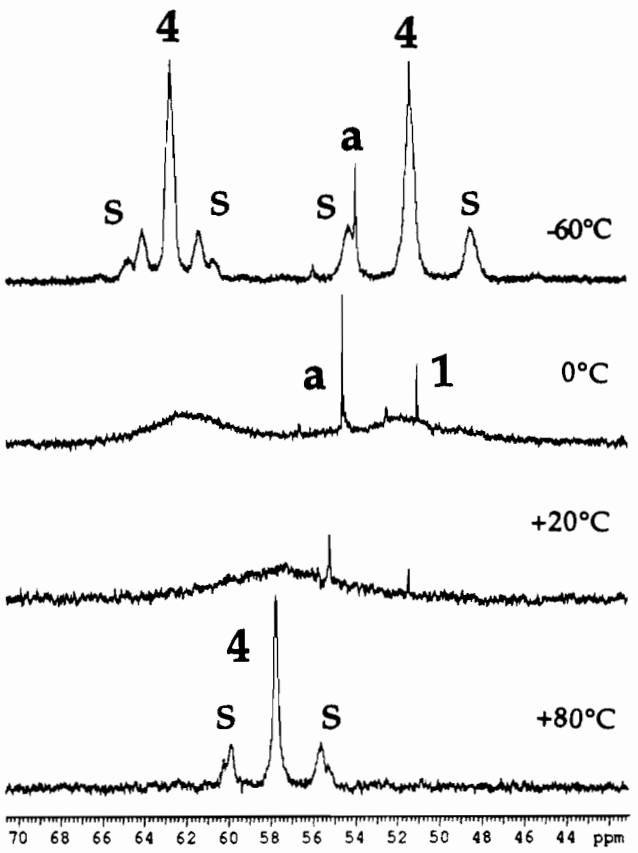

Figure 6. Variable temperature ^{31}P NMR spectra for $\mathbf{4(NO_3)_2}$ (T = +80 °C in DMSO solvent; T = +20 to −60 °C in CD_3OD solvent). The sharp peaks at δ 51.6 ppm and δ 55.4 ppm correspond to **1** and $[Pt(AuPPh_3)_8]^{2+}$ (**a**), respectively. S indicates ^{195}Pt and ^{199}Hg satellite peaks of **4**.

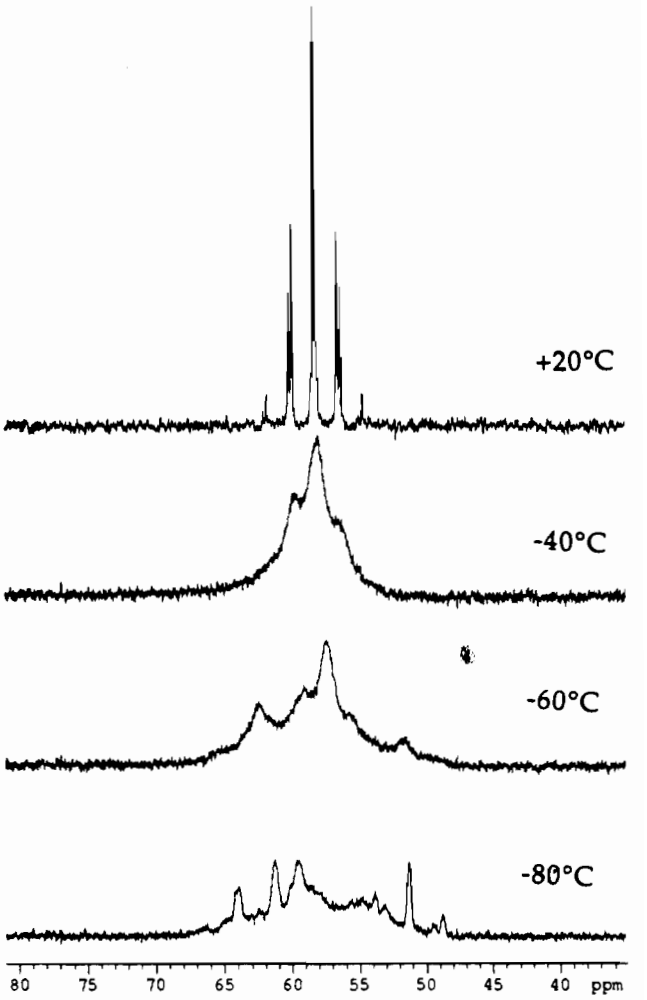

Figure 7. Variable temperature ^{31}P NMR spectra for $[(HgNO_3)_2Pt(AuPPh_3)_8](BF_4)_2$, $\mathbf{6(BF_4)_2}$, with acetone-d_6 as solvent. The spectrum at 20 °C is identical to the spectrum for this compound reported in the literature.[11]

was lowered. At 80 °C in DMSO solution, a fully coalesced resonance was observed at 57.7 ppm for **4** with ^{195}Pt and ^{199}Hg satellites (δ 57.7 ppm, $^2J_{^{195}Pt-P}$ 517 Hz, $^3J_{^{199}Hg-P}$ 601 Hz). Similar results were observed in the ^{31}P NMR for the Pd analog, **5**. The dynamic behavior observed in the ^{31}P NMR for **4** and **5** is consistent with two exchanging, chemically nonequivalent phosphorus environments. The two nonequivalent phosphorus environments result from the single Hg atom capping a square Au_4 face (see Figures 2 and 3 for **4**). Thus P1, P2, P3, and P4 represent one environment (on the side of the Hg atom) and P5, P6, P7, and P8 represent the other (on the side away from the Hg atom). The dynamic behavior results from a process that interchanges these two environments. The process is likely to involve intermolecular Hg exchange but this has not been studied further. The spectra in Figure 6 are in agreement with the various isotopomers and their calculated abundance.

$[(HgNO_3)_2Pt(AuPPh_3)_8]^{2+}$ (M = Pt, 6; Pd, 7). Eighteen-electron clusters of the general formulation $[(HgNO_3)_2M(AuPPh_3)_8]^{2+}$ were prepared in good yield by reaction of the 16-electron $[M(AuPPh_3)_8]^{2+}$ with 1 equiv of Hg_2^{2+} according to the procedure given in the literature for M = Pt.[11] The Pd-centered cluster **7** has not been previously synthesized. Cluster $\mathbf{6(BF_4)_2}$ was also prepared by the oxidation of **1** with 2 equiv of $HBF_4{\cdot}Et_2O$. Cluster $\mathbf{6(PF_6)_2}$ was prepared in a similar fashion by oxidation of **1** with 2 equiv of $[Fe(\eta^5\text{-}C_5H_5)_2]PF_6$. These oxidation reactions were followed by ^{31}P NMR and were observed to give **6** quantitatively (see Experimental Section).

In contrast to **1** and **2**, IR data for **6** and **7** in the solid state showed bands for bound NO_3^- (ca. 1260 cm^{-1}) in addition to uncoordinated NO_3^- (ca. 1350 cm^{-1}) (Table 5). Elemental analyses and ICP measurements confirmed the $[(HgNO_3)_2M(AuPPh_3)_8]^{2+}$ formulation. Equivalent conductance measurements (Λ = 299 mho cm^{-1} mol^{-1} for $\mathbf{6(NO_3)_2(BF_4)_2}$, Λ = 277 for $\mathbf{6(NO_3)_4}$, and Λ = 273 mho cm^{-1} mol^{-1} for $\mathbf{7(NO_3)_4}$) were indicative of two dissociated anions per cluster cation (Table 5). The ^{31}P NMR spectra recorded at different temperatures for **6** and **7** are shown in Figures 7 and 8. Note that **6** and **7** behaved like typical 18-electron cluster compounds,[1] showing complete stereochemical nonrigidity at ambient temperature and starting to freeze out only at very low temperatures. These spectra are very different from those of the 20-electron compounds **1**−**3** (Figure 4). The 20 °C spectra were successfully simulated as described in the literature for **6**[11] using the values of $^{195}Pt-P$ and $^{199}Hg-P$ coupling constants given in the Experimental Section.

The clusters $\mathbf{6(BF_4)_2}$ and $\mathbf{7(NO_3)_2}$ reacted with Cl^- to form $[(HgCl)_2M(AuPPh_3)_8]^{2+}$. In the case of $\mathbf{6(BF_4)_2}$, the resulting chloride adduct $[(HgCl)_2Pt(AuPPh_3)_8](BF_4)_2$ had spectroscopic properties identical to $[(HgCl)_2Pt(AuPPh_3)_8](NO_3)_2$ reported previously,[11] with the expected differences due to the different anions. The chloride adduct of **7** was characterized in solution by analogy to the chloride adduct of **6**. The resonance in the ^{31}P NMR for cluster **7** (δ 45 ppm) remained sharp upon the addition of 2 equivalents of Cl^- while the value of the coupling constant, $^3J_{^{199}Hg-P}$, decreased from 643 Hz to 516 Hz. The relative intensity of the Hg satellites indicated that the chloride adduct of **7** retained 2 Hg atoms. Similarly, the $^3J_{^{199}Hg-P}$ value for cluster **6** decreased on addition of Cl^- from 470 to 356 Hz.

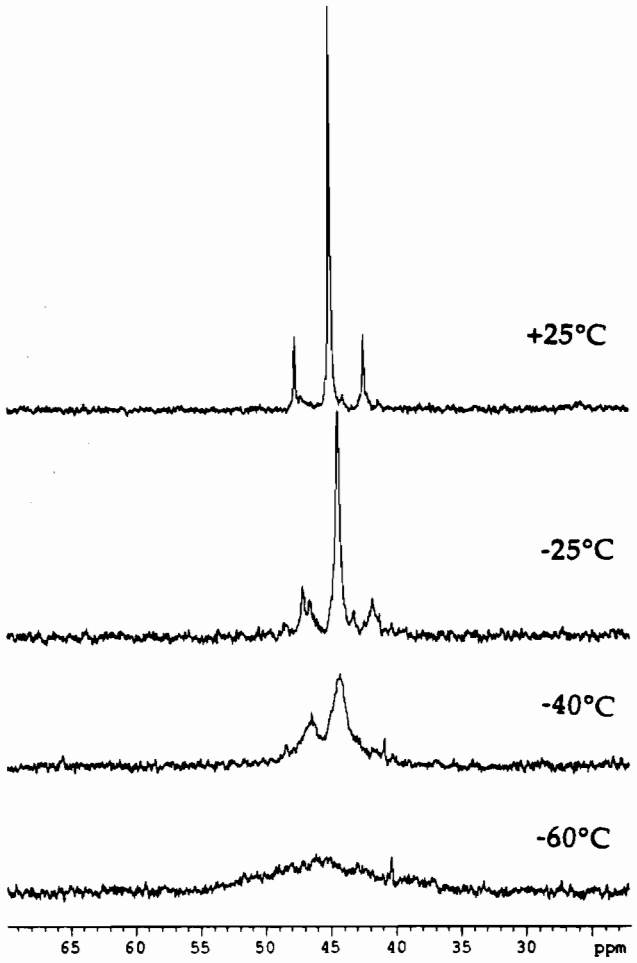

Figure 8. Variable temperature ^{31}P NMR spectra for $[(HgNO_3)_2Pd(AuPPh_3)_8](NO_3)_2$, **7**$(NO_3)_2$, with acetone-$d_6$ as solvent.

The strong Hg−Cl bond probably decreases the overall Hg−M−Au−P bonding causing the smaller $^3J_{^{199}Hg-P}$ values. $[(HgCl)_2Pd(AuPPh_3)_8]^{2+}$ was not isolated in the solid state and not characterized further.

Discussion

The first examples of 20-electron, metal-centered, gold cluster compounds have been synthesized by the reaction of $[M(AuPPh_3)_8]^{2+}$ (M = Pt, Pd) with metallic Hg. Clusters **1** and **2** were fully characterized by analytical and spectroscopic methods. The $[(Hg)_2M(AuPPh_3)_8]^{2+}$ cluster core formulation was confirmed for **2** in the solid state by single crystal X-ray analysis (Figure 1). The properties of these compounds are very different from those of the 18-electron clusters, $[(HgNO_3)_2M(AuPPh_3)_8]^{2+}$ (M = Pt, **6**; Pd, **7**), formed by the reaction of $[M(AuPPh_3)_8]^{2+}$ with Hg_2^{2+} salts. The 18-electron, monomercury clusters **4** and **5** were isolated as intermediates in the synthesis of **1** and **2**, respectively. These clusters were thoroughly characterized by analytical and spectroscopic methods and by single-crystal X-ray diffraction for **4** (Figures 2 and 3). Clusters **4** and **5** were converted into the 20-electron clusters **1** and **2**, respectively, by the addition of excess metallic Hg. In addition, solutions made from solid samples of **4** or **5** gave equilibrium amounts of $[M(AuPPh_3)_8]^{2+}$ and $[(Hg)_2M(AuPPh_3)_8]^{2+}$, showing that these Hg adducts are formed reversibly. Importantly, the 20-electron clusters **1** and **2** were cleanly transformed into their 2-electron oxidized, 18-electron analogs, **6** and **7**, by reaction with 2 equivalents of $Fe(\eta^5\text{-}C_5H_5)_2^+$. All of the transformations of the clusters in this study are shown in the Reaction Scheme I. An analogous 20-electron, Au-centered, (bis)mercury cluster, $[(Hg)_2Au(AuPPh_3)_8]^{3+}$, **3**, was also prepared by the reaction of metallic Hg with the 16-electron cluster $[Au(AuPPh_3)_8]^{3+}$.

The ^{31}P NMR spectra of clusters **1**−**3** recorded at various temperatures are shown in Figure 4 and need some discussion. The changes with temperature for all three clusters are similar and indicate fluxional behavior. At the lower temperatures (<0 °C), two sets of $^3J_{^{199}Hg-P}$ satellite doublets are observed. This is due to the magnetic non-equivalence of two distinct phosphorus sites in isotopomer (c) shown in Figure 5 and discussed in detail in the Experimental Section. As the temperature was increased, the two ^{199}Hg satellite doublets in **1**−**3** broadened and coalesced to a single, average doublet. The approximate temperatures of coalescence for clusters **1**, **2**, and **3** are +40, +20, and −10 °C, respectively. The fluxional process that causes this coalescence must average the magnetically nonequivalent phosphorus environments in isotopomer c by a nondissociative, skeletal rearrangement process. The dissociation of Hg, PPh_3, or $AuPPh_3$ species cannot cause this coalescence because $^{195}Pt-P$ and $^{199}Hg-P$ coupling is maintained and not decreased. Such rapid skeletal rearrangement in metal-centered Au clusters is common and has been discussed in several reviews.[1−3] It is interesting that the rate of this rearrangement increases in the order Pt < Pd < Au for the $Hg_2M(AuPPh_3)_8^{n+}$ clusters. The spectrum of **1** also showed the $^2J_{^{195}Pt-P}$ satellite doublet which broadened at lower temperatures, presumably due to the slowing of a separate fluxional process.

The reaction of the Pt-centered clusters **1** and **4** with 1 atm of CO resulted in the clean and rapid displacement of metallic Hg to give the stable, 18-electron, $[(CO)Pt(AuPPh_3)_8]^{2+}$. This reaction was not reversed under a N_2 purge. This type of a reaction has been observed before with $[(HgNO_3)(PPh_3)Pt(AuPPh_3)_6]^+$, which reacts with CO to give $[(CO)(PPh_3)Pt(AuPPh_3)_6]^+$ and metallic Hg.[13] In contrast, $[(Hg)Pd(AuPPh_3)_8]^{2+}$, **5**, reacted with CO reversibly, giving $[(CO)Pd(AuPPh_3)_8]^{2+}$. A N_2 purge completely reversed this reaction. Interestingly, **2** was unreactive toward 1 atm of CO. The Au-centered cluster $[(Hg)_2Au(AuPPh_3)_8]^{3+}$, **3**, also did not react with CO. This trend in reactivity with CO is due to the relative differences in the stability of the CO containing products $[(CO)M(AuPPh_3)_8]^{n+}$. The stability order for the central metal M is Pt > Pd ≫Au.[25,26]

The reactivity of the 20-electron cluster **1** with Cl^- was very different from its 18-electron analog **6**. Cluster **6** reacted stoichiometrically and cleanly with 2 equivalents of Cl^- ion to form $[(HgCl)_2M(AuPPh_3)_8]^{2+}$.[11] This cluster was soluble in polar solvents such as methanol, acetone, and dichloromethane; however, the reaction of **1** with 2 equivalents of Cl^- gave a product that was insoluble in dichloromethane and other polar and nonpolar solvents. FABMS analysis of this product was consistent with the formulation "$Hg_2Cl_2M(AuPPh_3)_8$" or an oligomer of this formulation (see Experimental Section). A suspension of this dichloride derivative of **1** reacted with $Fe(\eta^5\text{-}C_5H_5)_2^+$ to yield a solution that contained the 18-electron cluster $[(HgCl)_2M(AuPPh_3)_8]^{2+}$. These transformations are summarized in the Reaction Scheme I and provide additional evidence for the 20-electron formulation of **1** and its chloride adduct.

The bonding in high nuclearity M-centered cluster compounds has been described by Mingos et al. using a delocalized

(25) Kanters, R. P. F.; Schlebos, P. P. J.; Bour, J. J.; Bosman, W. P.; Smits, J. M. M.; Beurskens, P. T.; Steggerda, J. J. *Inorg. Chem.* **1990**, *29*, 324.
(26) Kanters, R. P. F.; Schlebos, P. P. J.; Bour, J. J.; Bosman, W. P.; Behm, H. J.; Steggerda, J. J. *Inorg. Chem.* **1988**, *27*, 4034.

molecular orbital model derived from Stone's tensor surface harmonic theory.[10,27,28] An electron-counting formalism derived from this theory has proven useful in predicting structure and rationalizing the reactivity of these M-centered, Au cluster compounds. This electron count is based on the number of electrons in bonding molecular orbitals of σ-type symmetry (there are four: S^{σ}, P_x^{σ}, P_y^{σ}, and P_z^{σ}) which point radially in toward the center of the cluster. The electron count of 20 for **1** and **2** is unusual and has not been observed previously. Since only 8 electrons are needed to fill the four bonding orbitals of σ symmetry indicated above, the two extra electrons in the 20-electron clusters **1** and **2** are probably located in nonbonding orbitals. In these clusters, the Hg atoms do not have coordinating ligands and therefore have orbitals pointing outward away from the cluster core. The "extra" electrons probably occupy nonbonding molecular orbitals which have large contributions from these Hg orbitals. In the 18-electron clusters **6** and **7**, the Hg atoms are coordinated by anions such as NO_3^- or Cl^- and do not have these nonbonding electron pair. Thus, while **1** and **2** *formally* count as 20-electron species their structural and bonding properties should be similar to their 18-electron analogs.

Preliminary studies of the electrochemistry and UV−vis absorption spectroscopy of the Pt-centered, Hg-Au clusters are in qualitative agreement with the results described above. For example, 2 electrons are reversibly added (by cyclic voltammetry) to 16-electron clusters such as $[M(AuPPh_3)_8]^{n+}$ where M = Au (n = 3), Pt or Pd (n = 2),[29] while 18-electron clusters such as $[(CO)Pt(AuPPh_3)_8]^{2+}$ show only irreversible electrochemistry.[1−3,29] A preliminary investigation of the electrochemistry of the 20-electron cluster $[(Hg)_2Pt(AuPPh_3)_8]^{2+}$, **1**, and the 18-electron cluster $[(HgNO_3)_2M(AuPPh_3)_8]^{2+}$, **6**, showed only irreversible processes very similar to other 18-electron clusters. The UV−vis absorption spectrum of **1** (CH_3CN solution) is also very similar to those of the 18-electron clusters **4**, $[(HgCl)_2Pt(AuPPh_3)_8]^{2+}$, and $[(CO)Pt(AuPPh_3)_8]^{2+}$ (Experimental Section). The spectra of 16-electron clusters is distinctly different from those of 18-electron clusters.[1,3,30] A complete analysis of the UV−vis absorption and magnetic circular dichroism spectra of these and related clusters is underway and should help in our understanding of the bonding in these interesting compounds.[31]

Experimental Section

Physical Measurements and Reagents. ^{31}P NMR spectra were recorded at 121.4 MHz with use of a Varian VXR-300 MHz spectrometer, and at 202.353 MHz with the use of a Varian VXR-500 MHz spectrometer. ^{31}P NMR spectra were run with proton decoupling and shifts are reported in ppm relative to internal standard trimethylphosphate (TMP) with positive shifts downfield. Infrared spectra were recorded in the solid state on a Perkin-Elmer Model 1600 FT-IR spectrometer or Galaxy Series 3000 FT-IR spectrometer with use of CsI pellets. Conductivity measurements were made with use of a Yellow Springs Model 35 conductance meter. Compound concentrations used in the conductivity experiments were 3×10^{-4} M in CH_3CN or acetone solution. FABMS measurements were carried out with the use of a VG Analytical, Ltd. 7070E-HF high resolution, double-focusing mass spectrometer equipped with a VG 11/250 data system. FABMS samples were introduced in a *m*-nitrobenzyl alcohol matrix. Microanalyses of compounds **1**, **3**, **4**, and **6** were carried out by Analytische Laboratories, Engelskirchen, Germany, and analyses of compounds **2**, **5**, and **7** by E + R Microanalytical Laboratory, Inc., Corona, NY. ICP analyses of DMSO solutions of the clusters were carried out with the use of a Plasma 200 ICP A-E spectrometer with $Pt(AuPPh_3)_8(NO_3)_2$ and $Pd(AuPPh_3)_8(NO_3)_2$ used as references.[30] Electronic absorption spectra were recorded with use of CH_3CN as solvent. Solvents were dried and distilled prior to use. The cluster compounds $[Pt(AuPPh_3)_8](NO_3)_2$,[15] $[Pt(AuPPh_3)_8](PF_6)_2$,[15] $[Pd(AuPPh_3)_8](NO_3)_2$,[16,17] $[Au(AuPPh_3)_8](NO_3)_3$,[32] $[(CO)Pt(AuPPh_3)_8](NO_3)_2$,[25,26] $[(HgCl)_2Pt(AuPPh_3)_8(NO_3)_2$,[11] and $[(HgNO_3)_2Pt(AuPPh_3)_8](NO_3)_2$[11] were prepared as described in the literature. All other chemicals were reagent grade (including Hg^0 and $[Hg(H_2O)(NO_3)]_2$) and were used without further purification. Unless otherwise noted, all manipulations were carried out under a purified N_2 atmosphere with standard Schlenk techniques.

^{31}P NMR Simulations. The ^{31}P NMR spectra of **1**−**3** (Figure 4) were successfully simulated with use of the VNMR program LAME (supplied with the Varian software package) as described below and illustrated in Figure 5 for cluster **1**. The chemical shift and J values used in the simulations are given below under the compound preparations. The ^{31}P NMR spectra are complicated in that two different J values were observed for $^{199}Hg-P$ coupling. Thus, although all of the phosphorus atoms are in chemically equivalent environments, the *magnetic* nonequivalence of the phosphorus sites in some of the isotopomers is observable. The ambient temperature ^{31}P NMR spectrum of **1** shown in Figure 5 provides a good example of this (see Figure 5 for a definition of the isotopomers and their relative populations). A sharp singlet was observed for isotopomer a in which the eight P atoms are in chemically and magnetically equivalent environments. A doublet (seen as sharp ^{195}Pt satellites) was observed for isotopomer b in which the eight equivalent P atoms couple to the central ^{195}Pt. Two broad sets of ^{199}Hg satellites were observed for isotopomer c due to the fact that the eight P atoms, while chemically equivalent with respect to the Hg atoms, are in magnetically nonequivalent positions (only one of the two Hg atoms is NMR active). Thus the four phosphines closest to the ^{199}Hg couple with a different J value than the four which are further away. Additional coupling to ^{195}Pt gave rise to two broad sets of doublets of doublets for isotopomer d and a sharp triplet was observed for isotopomer e in which the eight magnetically equivalent P atoms couple to the two $I = {}^1/_2$ ^{199}Hg atoms. The coupling pattern for isotopomer f in which all possible nuclei are spin active was not observed due to its low intensity. Simulations for **2** and **3** were similar to that of **1** except the $P-^{195}Pt$ coupling was absent.

Preparation and Characterization Data of Compounds. $[(Hg)_2Pt(AuPPh_3)_8](NO_3)_2$ ($\mathbf{1}(NO_3)_2$). One drop (ca. 80 mg) of metallic mercury was added to a stirred solution of $Pt(AuPPh_3)_8(NO_3)_2$ (65.3 mg, 0.0164mmol) in methanol (3 mL). The originally dark red/brown solution was stirred rapidly at room temperature for 4 h. The resulting bright red solution was filtered through diatomaceous earth to remove the unreacted Hg^0. The clear bright red filtrate was carefully layered in a test tube with 10 mL of diethyl ether. Large, polyhedral, red crystals resulted upon standing overnight. The crystals were collected, washed with 2 × 3 mL diethyl ether and allowed to air dry. Yield: 65.2 mg (0.0148 mmol), 91% based on Pt. The red solid was soluble in methanol, acetone, CH_3CN, pyridine, DMSO, and halogenated solvents and insoluble in saturated alkanes, diethyl ether, and THF. $^{31}P\{^1H\}$ NMR (methanol-d_4 20 °C) (Figures 4 and 5): δ 51.6 ppm (singlet with ^{195}Pt and broad ^{199}Hg satellites, $^2J_{^{195}Pt-P}$ 485 Hz, $^3J_{^{199}Hg-P}$ ca. 365 Hz and $^3J_{^{199}Hg-P}$ ca. 250 Hz). The spectra showed the same chemical shift and coupling constant values from +20 to −40 °C, with only slight sharpening of the ^{199}Hg satellites and broadening of the ^{195}Pt satellites. $^{31}P\{^1H\}$ NMR (DMSO-d_4, +60 °C): δ 51.6 ppm (singlet with ^{195}Pt and ^{199}Hg satellites $^2J_{^{195}Pt-P}$ 480 Hz, $^3J_{^{199}Hg-P}$ 300 Hz). FTIR: $\nu(NO_3)$ 1340 cm^{-1} (br, unbound). ICP: Pt:Au:P = 1.0:8.13:8.08. Anal. Calcd for $PtAu_8Hg_2P_8C_{144}H_{120}N_2O_6$ (mol wt 4394.33): C, 39.36; H, 2.75; N, 0.64. Found: C, 39.13; H, 2.83; N, 0.62. Equivalent conductance (acetone) = 313 mho cm^2 mol^{-1}. FABMS: obsvd *m/z*: {calcd 4394.3 for $[Pt(AuPPh_3)_8Hg_2(NO_3)_2 = M]^+$ unobserved}, 4131.3 {calcd 4131.7 for $[M - (HgNO_3)]^+$}, 3868.4 {calcd 3869.1 for $[M - 2(HgNO_3)]^+$}, 3668.5 {calcd 3668.8 for [M −

(27) Hall, K. P.; Mingos, D. M. P. *Prog. Inorg. Chem.* **1984**, *32*, 237.
(28) Mingos, D. M. P.; Watson, M. J. *Adv. Inorg. Chem.* **1992**, *39*, 327.
(29) van der Linden, J. G. M.; Roelofsen, A. M.; Ipskamp, G. H. W. *Inorg. Chem.* **1989**, *28*, 967. van der Linden, J. G. M.; Paulussen, M. L. H.; Schmitz, J. E. J. *J. Am. Chem. Soc.* **1983**, *105*, 1903.
(30) Schoondergang, M. F. J. Ph.D. Thesis (ISBN 9090049649), University of Nijmegen, Nijmegen, The Netherlands, 1992.
(31) Preliminary results: Mason, W. R. Northern Illinois University.
(32) Cook, C. D.; Jauhal, G. S. *J. Am. Chem. Soc.* **1968**, *90*, 1464.

$((Hg)_2NO_3PPh_3)]^+$}, 3606.5 {calcd 3606.8 for $[M - ((HgNO_3)_2PPh_3)]^+$}, 3406.4 {calcd 3406.6 for $[M - ((Hg)_2NO_32PPh_3)]^+$}, 3344.3 {calcd 3344.6 for $[M - 2(HgNO_3PPh_3)]^+$}, 3144.9 {calcd 3144.3 for $[M - ((Hg)_2NO_3(PPh_3)_3)]^+$}, 3082.4 {calcd 3082.3 for $[M - ((HgNO_3)_2(PPh_3)_3]^+$}. Two different crystalline forms were found for this cluster, both of which have a similar appearance. Unit cell data for both forms are as follows: form A, space group *P4/n*, $a = 17.656$ Å, $c = 22.812$ Å, $V = 7111$ Å^3; form B, space group *Fddd*, $a = 38.48(2)$ Å, $b = 41.20(2)$ Å, $c = 34.38(4)$ Å, $V = 54\,500$ Å^3. Crystals from both forms were unsuitable for complete structure analyses.

$[(Hg)_2Pt(AuPPh_3)_8](PF_6)_2$ ($\mathbf{1(PF_6)_2}$) was prepared by two methods.

Method A. Red crystals of $\mathbf{1(NO_3)_2}$ (50 mg, 0.011 mmol) were dissolved in 4 mL of methanol. To the stirred red solution was added 2 mL of a colorless methanol solution of Bu_4NPF_6 (88 mg, 0.23 mmol) was added. A red precipitate formed almost immediately. The suspension was allowed to stir for 10 min, at which time the solid was collected on a frit and washed with 1 mL of methanol and then 2 × 3 mL of diethyl ether. The red microcrystalline solid was allowed to air dry. Yield: 36 mg (0.0079 mmol), 70% based on Pt.

Method B. To a stirred dark brown solution of $[Pt(AuPPh_3)_8](PF_6)_2$ (65 mg, 0.016 mmol) in 8 mL of acetone was added 1 drop of Hg^0 (ca. 80 mg). The reaction mixture was stirred rapidly for 2 h, at which time the bright red solution was filtered through glass wool to remove the excess Hg^0. The bright red acetone filtrate was carefully layered with 25 mL of diethyl ether and allowed to stand overnight. A red microcrystalline powder was collected the next day, washed with 2 × 3 mL diethyl ether, and allowed to air dry. Yield: 40 mg (0.0088 mmol), 56% based on Pt. $\mathbf{1(PF_6)_2}$ was slightly soluble in methanol, soluble in acetone, acetonitrile, and dichloromethane and insoluble in diethyl ether, saturated hydrocarbons, and THF. $\mathbf{1(PF_6)_2}$ had the same spectroscopic properties as $\mathbf{1(NO_3)_2}$, except the NO_3^- stretch in the IR was replaced by $\nu(PF_6)$ 840 cm^{-1} and a septet was observed in the ^{31}P NMR for PF_6 at δ −146 ppm.

$[(Hg)_2Pd(AuPPh_3)_8](NO_3)_2$ ($\mathbf{2(NO_3)_2}$). One drop of metallic mercury (ca. 80 mg) was added to 4 mL of a methanol solution of $[Pd(AuPPh_3)_8](NO_3)_2$ (100 mg, 0.026 mmol). After being stirred for 30 min, the solution turned from dark red/brown to bright red. The solution was filtered through diatomaceous earth and the filtrate was evaporated to dryness under reduced pressure. The red residue was dissolved in 4 mL of methanol, and 20 mL of diethyl ether was added slowly with swirling until small crystals began to form. The flask was left undisturbed overnight. The resulting red crystalline solid was collected, washed with 2 × 3 mL of diethyl ether and air dried. Yield: 76 mg (0.018 mmol), 69% based on Pd. The dark red solid was soluble in dichloromethane, acetone, methanol, and nitromethane and insoluble in saturated hydrocarbons and diethyl ether. Recrystallization by liquid diffusion of diethyl ether into a concentrated methanol solution gave red prisms suitable for X-ray analysis. $^{31}P\{^1H\}$ NMR (acetone-d_6, 20 °C) (Figure 4): δ 44.9 ppm (singlet with ^{199}Hg satellites, $^3J_{^{199}Hg-P}$ 291 Hz). $^{31}P\{^1H\}$ NMR (acetone-d_6, −40 °C): δ 44.9 ppm (singlet with ^{199}Hg satellites, $^3J_{^{199}Hg-P}$ 219 Hz and $^3J_{^{199}Hg-P}$ 376 Hz). FTIR: $\nu(NO_3)$ 1363 cm^{-1} (br, unbound). ICP: Pd:Au:P = 1:8.07:8.12. Anal. Calcd for $PdAu_8Hg_2P_8C_{144}H_{120}N_2O_6$ (mol wt 4305.67): C, 40.16; H, 2.81; N, 0.65. Found: C, 39.24; H, 2.65; N, 0.66. Equivalent conductance (acetonitrile) = 304 mho cm^2 mol^{-1} . FABMS: obsvd *m/z*: {calcd 4305.7 for $[Pd(AuPPh_3)_8Hg_2(NO_3)_2 = M]^+$ unobserved}, 4042.5 {calcd 4043.1 for $[M - (HgNO_3)]^+$}, 3780.0 {calcd 3780.6 for $[M - 2(HgNO_3)]^+$}, 3579.8 {calcd 3580.2 for $[M - ((Hg)_2NO_3PPh_3)]^+$}, 3517.8 {calcd 3518.2 for $[M - ((HgNO_3)_2PPh_3)]^+$}, 3317.3 {calcd 3317.9 for $[M - ((Hg)_2NO_3(PPh_3)_2)]^+$}.

$[(Hg)_2Au(AuPPh_3)_8](NO_3)_3$ ($\mathbf{3(NO_3)_3}$). The green powder $[Au(AuPPh_3)_8](NO_3)_3$ (71.9 mg, 0.0177 mmol) was dissolved in 10 mL of freshly distilled methanol. One drop of metallic mercury (ca. 80 mg) was added to the stirred dark red solution. The reaction flask was covered with foil and the mixture rapidly stirred for 4 h. Reactions carried out under the room light resulted in the formation of Au^0 mirrors and lower yields. The solution became bright red and was reduced in volume to 6 mL and filtered through diatomaceous earth. In order to facilitate the rate of crystal growth, the filtrate was divided equally between two test tubes and each 3 mL aliquot of mother liquor layered carefully with 10 mL of diethyl ether. Small plate-like red crystals resulted on standing overnight in the refrigerator. The crystals were collected by decanting off the mother liquor and washing with 3 × 2 mL diethyl ether. Yield: 49 mg (0.011 mmol) 62% based on Au. The red solid was soluble in methanol, acetone, acetonitrile, dichloromethane and insoluble in saturated hydrocarbons, diethyl ether, and THF. $^{31}P\{^1H\}$ NMR (methanol-d_4, 20 °C) (Figure 4): δ 52.7 ppm (singlet with ^{199}Hg satellites $^3J_{^{199}Hg-P}$ 299 Hz). At low temperature the ^{199}Hg satellites decoalesced into two sharp sets of satellites {(methanol-d_4, −30 °C): δ 52.7 ppm $^3J_{^{199}Hg-P}$ 230 Hz and $^3J_{^{199}Hg-P}$ 368 Hz}. Integration of the ^{199}Hg satellites peak areas confirmed the presence of two Hg atoms (area of ^{199}Hg satellites/area of center peak = 0.47, calculated for two Hg per cluster = 0.40). FTIR: $\nu(NO_3)$ 1340 cm^{-1} (br, unbound). Equivalent Conductance (CH_3CN) = 378 mho cm^2 mol^{-1}. ICP: Au:P = 8.42:8 (**3** was only slightly soluble in DMSO which gave rise to an increased error in the ICP experiment). Anal. Calcd for $Au_9Hg_2P_8C_{144}H_{120}N_3O_9$ (mol wt 4582.2): C, 38.80; H, 2.71; N, 0.94. Found: C, 38.72; H, 2.65; N, 1.06. Only peaks corresponding to fragmentation of $[Au(AuPPh_3)_8]^{3+}$ were observed in the FABMS experiment.

$[(Hg)Pt(AuPPh_3)_8](NO_3)_2$ ($\mathbf{4(NO_3)_2}$). Method A. Red crystalline $\mathbf{1(NO_3)_2}$ (82.9 mg, 0.019 mmol) was dissolved in 6 mL of methanol. To the bright red solution was added solid $[Pt(AuPPh_3)_8](NO_3)_2$ (75.8 mg, 0.019 mmol), immediately yielding a dark, red-brown solution. The reaction mixture was allowed to stir for 4 h at which time the mixture was filtered through diatomaceous earth and the filtrate divided into two test tubes. The dark solution (3 mL) in each test tube was carefully layered with 15 mL of diethyl ether. Very dark, red-black crystals formed on standing overnight. The crystals were collected by decanting off the mother liquor and washed with 3 × 2 mL of diethyl ether. Yield: 146.0 mg (.035 mmol), 92% based on Pt.

Method B. The same procedure for preparation of $\mathbf{1(NO_3)_2}$ was followed with the exception of reaction time. The reaction mixture was stopped after approximately 1 h (while it was still dark red-brown in color) and layered as directed above. Yields for this method varied depending on the point at which the reaction was terminated. Often a mixture of red crystals of **1** and dark red/black crystals of **4** formed. The dark solid was soluble in methanol, acetone, CH_3CN, DMSO, and halogenated solvents and insoluble in saturated alkanes, diethyl ether, and THF. $^{31}P\{^1H\}$ NMR (methanol-d_4, 20 °C) (Figure 6): broad resonance centered at δ 57.6 ppm corresponding to **4** and two sharp singlets (δ 51.58 ppm and $^2J_{^{195}Pt-P}$ 485 Hz and δ 55.4 ppm $^2J_{^{195}Pt-P}$ 495 Hz) corresponding to equilibrium amounts of $[Pt(AuPPh_3)_8]^{2+}$ and **1**. At higher temperature, the broad signal sharpened to a singlet with ^{195}Pt and ^{199}Hg satellites {(DMSO-d_6, +80 °C): δ 57.7 ppm, $^2J_{^{195}Pt-P}$ 517 Hz, $^3J_{^{199}Hg-P}$ 601 Hz}. At low temperature, the signal decoelesced to two singlets with ^{195}Pt and ^{199}Hg satellites {(acetone-d_6, −60 °C): δ 62.6 ppm, $^2J_{^{195}Pt-P}$ 330 Hz, $^3J_{^{199}Hg-P}$ 480 Hz; δ 51.5 ppm, $^2J_{^{195}Pt-P}$ 704 Hz, $^3J_{^{199}Hg-P}$ 704 Hz} each integrating for 50% of the signal, thus indicating two chemically nonequivalent phosphorus environments. FTIR: $\nu(NO_3)$ 1340 cm^{-1} (br, unbound). Equivalent conductance (CH_3CN) = 312 mho cm^2 mol^{-1}. ICP: Pt:Au:P = 1:8.08:8.09. Anal. Calcd for $PtAu_8HgPC_{144}H_{120}N_2O_6$ (mol wt 4193.7): C,41.24 ; H, 2.88; N, 0.67. Found: C, 40.86; H, 2.89; N, 0.70. FABMS: obsvd *m/z*: {calcd 4193.7 for $[Pt(AuPPh_3)_8(Hg)(NO_3)_2 = M]^+$ unobserved}, 4131.2 {calcd 4131.7 for $[M - (NO_3)]^+$}, 3868.8 {calcd 3869.1 for $[M - (Hg(NO_3)_2)]^+$}, 3668.4 {calcd 3668.8 for $[M - (NO_3HgPPh_3)]^+$}, 3606.5 {calcd 3606.8 for $[M - (Hg(NO_3)_2PPh_3)]^+$}, 3406.2 {calcd 3406.6 for $[M - (HgNO_3(PPh_3)_2)]^+$}, 3344.1 {calcd 3344.6 for $[M - (Hg(PPh_3)_2(NO_3)_2)]^+$}.

$[(Hg)Pd(AuPPh_3)_8](NO_3)_2$ ($\mathbf{5(NO_3)_2}$). To 2 mL of a red methanol solution of $\mathbf{2(NO_3)_2}$ (40 mg, 0.0093 mmol) was added 5 mL of a brown methanol solution of $[Pd(AuPPh_3)_8](NO_3)_2$ (38 mg, 0.0093 mmol). After being stirred for 20 min, the resulting dark red solution was filtered through diatomaceous earth and the solvent removed under reduced pressure. The residue was crystallized by dissolving the residue in 2 mL of methanol and layering with 20 mL of diethyl ether, resulting in dark red prisms. Yield: 26 mg (0.0063 mmol), 34% based on Pd. The red solid was soluble in dichloromethane, acetone, methanol, acetonitrile, and nitromethane and insoluble in saturated hydrocarbons and diethyl ether. $^{31}P\{^1H\}$ NMR (acetone-d_6, 20 °C): δ 47.7 ppm (singlet with ^{199}Hg satellites, $^3J_{^{199}Hg-P}$ 514 Hz). As with **4**, this resonance decoalesced at lower temperature into two broad singlets of equal intensity indicative of two nonequivalent phosphorus environ-

ments. $^{31}P\{^1H\}$ NMR (acetone-d_6, −40 °C): δ ca. 46.4 ppm and δ ca. 47.3 ppm (^{199}Hg satellites were unobserved). FTIR: $\nu(NO_3)$ 1357 cm^{-1} (br, unbound). ICP: Pd:Au:P = 1:8.03:7.83. Anal. Calcd for $PdAu_8Hg_2P_8C_{144}H_{120}N_2O_6$ (mol wt 4105.1): C, 42.12; H, 2.95; N, 0.68. Found: C, 41.97; H, 2.96; N, 0.70. Equivalent conductance (acetonitrile) = 304 mho cm^2 mol^{-1}. FABMS: obsvd *m/z*: {calcd 4105.1 for $[Pd(AuPPh_3)_8Hg(NO_3)_2 = M]^+$ unobserved}, 4042.7 {calcd 4043.1 for $[M - (NO_3)]^+$}, 3780.0 {calcd 3780.5 for $[M - (Hg(NO_3)_2)]^+$}, 3579.8 {calcd 3580.2 for $[M - (HgNO_3PPh_3)]^+$}, 3517.8 {calcd 3518.2 for $[M - (Hg(NO_3)_2PPh_3)]^+$}, 3317.3 {calcd 3317.9 for $[M - (Hg(PPh_3)_2NO_3)]^+$}.

$[(HgNO_3)_2Pt(AuPPh_3)_8](BF_4)_2$ ($6(BF_4)_2$). The NO_3^- and PF_6^- salts of **6** (**$6(NO_3)_2$** and **$6(PF_6)_2$**) were prepared as reported in the literature.[11] An alternative synthesis of **6** from **1** has also been used. Red crystalline **$1(NO_3)_2$** (50 mg, 0.011 mmol) was dissolved in 5 mL of distilled and degassed methanol. To the resulting clear red solution, 2 mol equiv of 85% $HBF_4{\cdot}Et_2O$ (0.004 mL, 0.027 mmol) were added *via* syringe. It is important to add just 2 equivalents of HBF_4 as addition of excess HBF_4 (e.g., 10 equiv) resulted in immediate metathesis and precipitation of **1** as the BF_4^- salt (**$1(BF_4)_2$**). The bright red solution turned more orange in color with stirring. After 1 h of stirring, the reaction mixture was allowed to stand undisturbed overnight. Small red crystals resulted which were collected, washed with 3 × 2 of mL diethyl ether, and allowed to air dry. Yield: 41 mg (0.0090 mmol), 79%. The red solid was slightly soluble in methanol, soluble in acetone, dichloromethane, and acetonitrile, and insoluble in saturated hydrocarbons, diethyl ether, and THF. $^{31}P\{^1H\}$ NMR (acetone-d_6, 20 °C): δ 58.4 ppm (singlet with sharp ^{195}Pt and ^{199}Hg satellites, $^2J_{^{195}Pt-P}$ 406 Hz, $^3J_{^{199}Hg-P}$ 470 Hz). The ^{31}P NMR data for **$6(NO_3)_2(BF_4)_2$** was the same as for the other salts of **6** reported in the literature.[11] The ^{31}P NMR spectra of **6** recorded as a function of temperature is shown in Figure 7. FTIR: $\nu(NO_3)$ 1260 cm^{-1} (bound), $\nu(BF_4)$ 1040 cm^{-1}. Equivalent conductance (acetone) = 299 mho cm^2 mol^{-1}. FABMS: obsvd *m/z*: {calcd 4567.9 for $[Pt(AuPPh_3)_8Hg_2(NO_3)_2(BF_4)_2 = M]^+$ unobserved}, 4481.3 {calcd 4481.1 for $[M - (BF_4)]^+$}, 4419.3 {calcd 4419.1 for $[M - ((BF_4)(NO_3))]^+$}, 4131.4 {calcd 4131.7 for $[M - (HgNO_3(BF_4)_2)]^+$}, 3959.6 {calcd 3959.5 for $[M - (AuHg(NO_3)_2BF_4)]^+$}, 3669.7 {calcd 3669.1 for $[M - (Hg(BF_4)_2(PPh_3)_2)]^+$}, 3409.1 {calcd 3409.8 for $[M - ((HgNO_3)_2(BF_4)_2AuPPh_3)]^+$}, 3344.8 {calcd 3344.5 for $[M - ((HgNO_3)_2(BF_4)_2(PPh_3)_2)]^+$}, 3147.5 {calcd 3147.6 for $[M - ((HgNO_3)_2(BF_4)_2Au(PPh_3)_2)]^+$}.

$[(HgNO_3)_2Pd(AuPPh_3)_8](NO_3)_2$ ($7(NO_3)_2$). Solid $[Hg(H_2O)(NO_3)]_2$ (16 mg, 0.0285 mmol) was added to a brown solution of $[Pd(AuPPh_3)_8](NO_3)_2$ (100 mg, 0.0256 mmol) in 6 mL of dry acetone. With stirring at 35 °C for 30 min, a red solution resulted which was filtered through diatomaceous earth, and the filtrate was evaporated to dryness under reduced pressure. The product was recrystallized by dissolving the residue in 2 mL of acetone and layering with 15 mL of diethyl ether. The resulting red needles were collected, washed with 2 × 3 of mL diethyl ether, and allowed to air dry. Yield: 63 mg (0.0142 mmol), 56%. The red crystals were soluble in dichloromethane and acetone, slightly soluble in methanol and acetonitrile, and insoluble in saturated hydrocarbons and diethyl ether. $^{31}P\{^1H\}$ NMR (acetone-d_6, 20 °C): δ 45.0 ppm (singlet with ^{199}Hg satellites $^3J_{^{199}Hg-P}$ 643 Hz). The variable temperature ^{31}P NMR spectra are shown in Figure 8. FTIR: $\nu(NO_3)$ 1265 and 1465 cm^{-1} (bound), 1350 cm^{-1} (br, unbound). Equivalent conductance (CH_3CN) = 273 mho cm^2 mol^{-1}. FABMS: obsvd *m/z*: {calcd 4429.7 for $[Pd(AuPPh_3)_8Hg_2(NO_3)_4 = M]^+$ unobserved}, 4043.2 {calcd 4043.1 for $[M - (Hg(NO_3)_3)]^+$}, 3780.7 {calcd 3780.5 for $[M - ((Hg)_2(NO_3)_4)]^+$}, 3518.3 {calcd 3518.2 for $[M - ((Hg)_2(NO_3)_4PPh_3)]^+$}, 3318.7 {calcd 3317.9 for $[M - ((Hg)_2(NO_3)_3(PPh_3)_2)]^+$}.

Reactions of 1, 2, 4, and 5 with CO. A methanol solution of the Pt-centered cluster **1** formed $[(CO)Pt(AuPPh_3)_8]^{2+}$ immediately when CO (1 atm) was bubbled through the solution. The reaction was carried out in an NMR tube, and metallic Hg was readily observed at the bottom of the tube. The reaction was irreversible due to the thermodynamic stability of $[(CO)Pt(AuPPh_3)_8]^{2+}$. The Pd-centered cluster **2** was unreactive toward CO. Both **4** and **5** reacted with CO to form $[(CO)M(AuPPh_3)_8]^{2+}$. As with **1**, $[(CO)Pt(AuPPh_3)_8]^{2+}$ formed irreversibly and Hg^0 was visible in the reaction vessel. Cluster **5** on the other hand reacted reversibly with CO forming $[(CO)Pd(AuPPh_3)_8]^{2+}$. This is demonstrated by the series of spectra in Figure 1S of the supplementary material. As described above, the monomercury cluster **5** (δ 47.7 ppm) is in equilibrium with the bis(mercury) cluster **2** (δ 44.9 ppm) and $[Pd(AuPPh_3)_8]^{2+}$ (δ 48.8 ppm) in solution (spectrum a). When CO(g) was bubbled through this solution, the peak at δ 47.7 ppm corresponding to **5** disappeared while a new peak at δ 44.5 ppm grew in corresponing to $[(CO)Pd(AuPPh_3)_8]^{2+}$. At the same time, the peak for **2** at δ 44.9 ppm increased in intensity (spectrum b). When the CO was removed from the solution under a stream of N_2, the peak corresponding to $[(CO)Pd(AuPPh_3)_8]^{2+}$ disappeared and the other peaks returned to their original intensity (spectrum c).

Reactivity of $1(NO_3)_2$ with Cl^-. To a stirred solution of **$1(NO_3)_2$** (44.9 mg 0.0102 mmol) in 3 mL of methanol was added 11.7 mg (0.0204 mmol) of solid $(PPh_3)_2NCl$. The bright red reaction mixture gradually became cloudy after 20 min of stirring. After 1 h of reaction time, the dull orange precipitate was collected on a frit and washed with 2 × 3 of mL Et_2O before drying *in vacuo*. Yield: 22.8 mg of a dull orange powder. The same reaction occurred with use of KCl as the source of Cl^- with the exception that the reaction was slower due to the lower solubility of solid KCl in methanol. The orange powder was insoluble in both polar and nonpolar solvents: acetone, methanol, dichloromethane, acetonitrile, nitrobenzene, nitromethane, *m*-nitrobenzyl alcohol, water, DMSO, THF, diethyl ether, pentane, and toluene. Due to its insolubility, ^{31}P NMR spectra and conductance measurements could not be obtained. FTIR: no stretches for NO_3^- (bound or uncoordinated) were found. FABMS (suspension in *m*-nitrobenzyl alcohol matrix): obsd *m/z*: {calcd 4341.2 for $[Pt(AuPPh_3)_8(Hg)_2(Cl)_2 = M]^+$ unobserved}, 3881.4 {calcd 3881.9 for $[M - (AuPPh_3)]^+$}, 3868.5 {calcd 3869.1 for $[M - 2(HgCl)]^+$}, 3606.6 {calcd 3606.8 for $[M - (HgCl)_2(PPh_3)]^+$}. The addition of an excess of $[Fe(\eta^5\text{-}C_5H_5)_2]PF_6$ to a suspension of this insoluble orange powder caused the solid to dissolve. ^{31}P NMR analysis of the resulting solution showed the presence of **6** and $[(HgCl)_2Pt(AuPPh_3)_8]^{2+}$ reported previously.[11]

Reaction of 1 with $[Fe(\eta^5\text{-}C_5H_5)_2]PF_6$. To 0.4 mL of an acetone solution of **$1(NO_3)_2$** (11.7 mg 0.00266 mmol) was added 0.2 mL of an acetone solution of 1.8 mg (0.0054 mmol) of $[Fe(\eta^5\text{-}C_5H_5)_2]PF_6$. The reaction was carried out in an NMR tube and ^{31}P NMR analysis showed immediate and clean conversion to **$6(NO_3)_2(PF_6)_2$**. This reaction is identical to that carried out with $HBF_4{\cdot}Et_2O$. See the preparation of **$6(NO_3)_2(BF_4)_2$** for spectroscopic details.

UV−Vis Absorption Spectra (CH_3CN solution) λ_{max} (nm) [log ϵ ($M^{-1}cm^{-1}$)]: for **1**, 441 [4.26 sh], 424 [4.37], 395 [4.40 sh], 340 [4.58 sh], 307 [4.92 sh], 286 [5.04]; for **4**, 483 [4.02], 406 [4.29], 377 [4.34 sh], 346 [4.55 sh], 313 [4.81 sh], 293 [4.99]; for $[(HgCl)_2Pt(AuPPh_3)_8]^{2+}$, 475 [3.73 sh], 433 [4.15 sh], 399 [4.46], 383 [4.48], 352 [4.48 sh], 293 [4.94 sh]; for $[(CO)Pt(AuPPh_3)_8]^{2+}$: 433 [3.23], 354 [4.26 sh], 315 [4.78 sh], 296 [4.92 sh], 284 [4.96].

Structural Determinations of $[(Hg)_2Pd(AuPPh_3)_8](NO_3)_2$ ($2(NO_3)_2$) and $[(Hg)Pt(AuPPh_3)_8](NO_3)_2$ ($4(NO_3)_2$). Collection and Reduction of Data. A summary of crystal data for **2** and **4** is presented in Table 1. Both crystals rapidly lost solvent at room temperature which rendered them unsuitable for X-ray diffraction. The crystals selected for data collection were therefore sealed in glass capillaries with a small amount of solvent vapor. In each case, the crystal class and space group was unambiguously determined by the Enraf-Nonius CAD4 peak search, centering, and indexing programs;[33] successful solution and refinement of the structures provided verification (vide infra). Intensity data were collected by using monochromatized Mo Kα radiation (λ = 0.710 69 Å). A total of 8424 reflections were collected for **2** of which 4945 were unique (R_{int} = 0.256); and 1777 reflections were considered as observed with $I > 2.0\sigma(I)$. In the case of cluster **4**, a total of 17 566 reflections were collected of which 16 845 were unique (R_{int} = 0.253) and 7504 were considered as observed with $I > 2.0\sigma(I)$. The intensities of three standard reflections were measured every 1.5 h of X-ray exposure time during data collection, and no decay was noted. The data were corrected for Lorentz, polarization, and background effects. An empirical absorption correction was applied by use of the program DIFABS.[34] All data were collected using an Enraf-Nonius CAD-4 diffractometer with controlling hardware and software,[33] and all

(33) Schagen, J. D.; Straver, L.; van Meurs, F.; Williams, G. Enraf-Nonius Delft, Scientific Instruments Division, Delft, The Netherlands, 1988.
(34) Walker, N.; Stuart, D. *Acta Crystallogr.* **1983**, *A39*, 158.

calculations were performed using the Molecular Structure Corp. TEXSAN crystallographic software package,[35] run on a Microvax 3 computer.

Solution and Refinement of Structures. Both structures were solved by direct methods.[36,37] Full-matrix least-squares refinement and difference Fourier calculations were used to locate the remaining non-hydrogen atoms. The atomic scattering factors were taken from the usual tabulation[38] and the effects of anomalous dispersion were included in F_c by using Cromer and Ibers' values of $\Delta f'$ and $\Delta f''$.[39] The palladium, platinum, mercury, and gold atoms were refined with anisotropic thermal parameters. The phosphorus atoms in **4** were also refined with anisotropic thermal parameters. The phosphorus atoms in **2** were refined isotropically. The phenyl carbon atoms were refined as rigid groups with fixed geometry. The orientations and temperature factors of these groups were allowed to refine. Rigid group refinement of phenyl rings is often used with large clusters of this type as disorder in the ligands is common and has little effect on the geometry of the metal core. Phenyl hydrogen atoms were included in their idealized positions. The final positional and thermal parameters of the refined atoms in clusters **2** and **4** are given in Tables 2 and 4, and the supplementary material.[12] ORTEP drawings of the cluster cores of **2** and **4** including the labeling schemes are shown in Figures 1−3. Distances and angles for **2** and **4** are given as supplementary material.[12]

(35) All calculations were carried out with use of the Molecular Structure Corporation *TEXSAN-TEXRAY Structure Analysis Package*, version 2.1, 1985.
(36) MITHRIL (an integrated direct methods computer program; University of Glascow, Scotland): Gilmore, C. J. *J. Appl. Crystallogr.* **1984**, *17*, 42.
(37) DIRDIF (Direct Methods for Difference Structures; an automatic procedure for phase extension and refinement of difference structure factors): Beurskens, P. T. *Technical Report 1984/1*, Crystallography Laboratory, Toernooiveld: 6525 ED Nijmegen, The Netherlands.
(38) Cromer, D. T.; Waber, J. T. In *International Tables for X-Ray Crystallography*; Kynoch: Birmingham, England, 1974; Vol. IV, Table 2.2 A.
(39) Cromer, D. T. In *International Tables for X-Ray Crystallography*; Kynoch: Birmingham, U.K., 1974; Vol. IV, Table 2.3.1. Ibers, J. A.; Hamilton, W. C. *Acta Crystallogr.* 1964, *17*, 781.

Acknowledgment. This work was supported by the National Science Foundation (Grant CHE-9222411) and by the University of Minnesota. J.W. acknowledges the University of Minnesota Undergraduate Research Opportunity Program for support.

Supplementary Material Available: Tables SI−SVI, listing final positional and thermal parameters for all atoms, general temperature factor expressions, and distances and angles and Figure S1, showing ^{31}P NMR spectra for the reaction of compound **5** with CO (43 pages).

IC9500366